Experimental modeling of bed morphological changes and toe erosion of emerged breakwaters due to wave-structure interactions in a deltaic coast

Nguyet-Minh Nguyen[1], Duong Do Van[1], Duy Tu Le[1], Quyen Nguyen[2], Nhat Truong Pham[3, 4], Ahad Hasan Tanim[5], Alexandre S. Gagnon[6], David P. Wright[7], Phong Nguyen Thanh[8,9,] Duong Tran Anh[8,9*]

[1] *Southern Institute of Water Resources Research, Ho Chi Minh City, Vietnam.*

[2] *Water Engineering and Management, Asian Institute of Technology, Phathum Thani, Thailand 12120.*

[3] *Division of Computational Mechatronics, Institute for Computational Science, Ton Duc Thang University, Ho Chi Minh City, Vietnam;*

[4] *Faculty of Electrical and Electronics Engineering, Ton Duc Thang University, Ho Chi Minh City, Vietnam;*

[5] *Department of Civil and Environmental Engineering, University of South Carolina, SC 29208, USA;*

[6] *School of Biological and Environmental Science, Liverpool John Moores University, Liverpool L3 3AF, United Kingdom*

[7] *Independent Researcher, Melbourne, Australia*

[8] *Institute for Computational Science and Artificial Intelligence, Van Lang University, Ho Chi Minh City, Vietnam*

[9] *Faculty of Environment, Van Lang University, Ho Chi Minh City, Vietnam*

* *Corresponding author: Van Lang University*

Email: duong.trananh@vlu.edu.vn (Duong T.A)

Abstract

Large-scale coastal erosion in the Mekong Delta has been dramatically increasing in severity in recent decades. There are several effective hard engineering solutions that have been implemented in this delta to efficiently prevent coastal erosion and stimulate sedimentation while supporting the local ecosystem conservation. These measures include Pile-Rock Breakwaters (PRBW), Hollow Triangle Breakwaters (HTB) and Semicircular Breakwaters (SBW). However, research on the sediment transport, morphological changes and toe erosion for these offshore breakwaters is very limited and is currently in the initial stages of understanding the specific conditions of sediment characteristics and foundations. The objective of this study was to reproduce the morphological changes and toe erosion of three breakwaters due to wave-structure interactions. This was investigated using 2D physical models with 3000 irregular waves during 8 experimental hours (equal to 15,000*T_p). To extract the bed morphological changes and toe erosion both specialized laser measurements (SW50M laser ruler) and analysis of high-speed video recording by images digitalization were applied. The experimental results show that the shape and structural design of offshore breakwaters can have a significant influence on the bed morphology on both the seaside and the leeside. We found that generally the toe of the construction on the seaside was eroded due to the occurrence of reflected waves, and that the flow is narrowed while passing through the construction, increasing the flow velocity and causing toe erosion. Additionally, the accretion of sediment at the leeside of the breakwaters was found to be mainly driven by the transport of sediment through the construction. Comparing the breakwater designs the experimental results showed that the HTB has the maximum accretion rate behind the structure, as well as the fastest accretion rate behind the breakwater. The SBW has high wave energy dissipation efficiency, although the toe erosion rate is faster than the other classes of breakwaters.

The PRBW shows the fastest toe erosion rate in front of the structure and causes accretion at the leeside of the construction but at a lower rate than the HTB. The findings from this study will help practical designers to reinforce the foot of construction during real breakwater designing and inform stability calculations. We recommendation is to apply these three classes of breakwaters, especially the HTB and SBW, for stimulating sedimentation for mangrove restoration in the mangrove mud-coast delta.

Key words: Toe erosion, bed morphological change, wave-structure interaction, physical model, Mekong Delta.

1. Introduction

The world's lowland deltas and mangrove mud-coasts are being severely eroded due to a range of factors including the effects of incident waves, storm-surge, and climate change induced sea-level rise (Luijendijk et al., 2018; Albers and Schmitt, 2015; Minderhoud et al., 2017; Winterwerp et al., 2020). This erosion leads to severe consequences such as land loss and subsidence, degradation of mangroves, and loss of coastal ecosystems (Giri et al., 2011; Lovelock et al., 2015; Winterwerp et al., 2020). Generally, the key drivers maintaining the sediment balance on deltaic coastlines is upstream river flow and downstream coastal sedimentation from the sea (Thanh et al., 2017; Le Xuan et al., 2019). Natural and human activities have significantly altered the coastline of these deltas in both the short and long term (Williams et al., 2018; Evans, 2012; Le Xuan et al., 2020, Mentaschi et al., 2018).

The Vietnamese Mekong Delta (VMD) is an important socioeconomic lowland area and is facing a range of challenges related to erosion. These include a rapid rate of subsidence

(Minderhoud et al., 2020), severe coastal erosion (Anthony et al., 2015) due to the reduction of upstream river sediment supply (Kondolf et al., 2014; Van Binh et al., 2020), uncontrolled riverbed mining (Li et al., 2017), conversion of mangrove forests into aquaculture ponds (Winterwerp et al., 2020), and climate change induced sea-level rise.

To adapt to this challenging situation, there are several hard engineering solutions that have been implemented in the VMD including construction of offshore breakwaters. Offshore breakwaters are coastal structures that reduce the impacts of incoming waves, currents, tides, and storms in coastal zones and are therefore effective at diminishing coastal erosion (Dai et al., 2018; Fitri et al., 2019). However, the construction of breakwaters can also change coastal morphology (Zyserman and Johnson, 2002; Klonaris et al., 2020) and can result in large-scale sediment erosion or accretion (Fitri and Yao, 2019). This alternation to the natural coastal morphology causes local changes to nearshore flow hydrodynamics (Fitri et al., 2019) and an imbalance of sediments over the entire coastline of the VMD. This means that the long-term stabilization of the coastline as well as the protection of the shoreline from wave and storms is an important consideration when designing breakwater solutions. Ideally, these breakwaters should not alter the bordering coastline or spread the sediment erosion or accretion issues adjacent locations.

Over time interactions between the coastal breakwaters and incoming waves can result in structural instability requiring frequent maintenance. On sandy and mud coasts, wave action is known to cause erosion of the breakwater's toe, which can result in structural failure. Fine sediment (i.e. sand, silt, mud) can also collect at the toe of the breakwater, filling the gaps inside the structure and diminishing its effectiveness as a wave dissipator and further contributing to the potential instability of the breakwater structure (Baquerizo and Losada, 1999). Therefore, the determination of toe erosion and accretion rate play important role in breakwater design and maintenance. A

variety of studies have been conducted to evaluate breakwater wave-structure interactions to understand toe erosion and bed morphological changes. For example, Baquerizo and Losada. (1999) explained the existence of erosion/deposition patterns at the foot of the construction by studying the formation of bars in front of the structure and the sediment transport at the toe of the structure. Zyserman and Johnson. (2002) provided a numerical model to investigate the impact of various breakwater layouts on erosion/deposition. Several breakwater layouts were investigated in a series of tests, in which the incident wave conditions were taken as constant in time. The results of these morphological simulations were found to agree qualitatively with field observations and predictions from empirical analysis.

Numerical modelling has provided a deeper understanding of bed morphological changes due to breakwaters. Ding et al. (2006) employed integrated numerical models to simulate irregular wave deformations, wave-induced currents, sediment transport, and morphodynamic changes around detached coastal breakwaters. These results showed an advancement in the ability to simulate waves and currents in a coastal zone with complex shorelines. Moreover, Birben et al. (2007) conducted experimental and numerical modeling to investigate the effects of offshore breakwater parameters and wave parameters on the sediment accumulation ratio. The results showed that the distance between the breakwater and the shoreline is one of the most important factors impacting the variation of sediment accumulation ratio for offshore breakwaters. In addition, Fitri et al. (2019) investigated the sediment transport and erosion-deposition patterns of a detached low-crested breakwater designed to protect the cohesive shoreline. The study used numerical modelling to understand the impacts of the breakwater on the nearshore hydrodynamics. The results of the analysis showed that the detached breakwater reduced both current speed and wave height behind the structure and the numerical results were also consistent with the field

measurements. Research by Ding and Wang (2008) on an integrated model of coastal and estuarine morphological processes was developed to simulate coastal and estuarine morphological processes. The successful application of the model to a medium-sized estuary and the numerical results of hydrodynamics and morphological changes indicate that the numerical model has the ability to simulate complicated coastal morphodynamics. Furthermore, Du et al. (2010) used COAST2D and associated model applications to investigate the effect of overtopping waves on the hydrodynamics and morphodynamics around a group of shore-parallel breakwaters. The hydrodynamic aspects of the model were validated against a series of laboratory conditions. The model results were compared with laboratory data and field measurements, showing a good agreement on both hydrodynamics and morphological changes. Finally, Hieu et al. (2020) undertook a study based on the SWASH wave model combined with a sediment transport model, the numerical results showed good agreement with the experimental data in the laboratory.

There are some notable studies using VMD case studies which include Thanh et al. (2017) who analyzed the dynamics of suspended sediment to investigate the relationship between different processes and flux pattern changes. The study applied a numerical model on two scales, comprising a large-scale model (the whole VMD) and a smaller-scale model (tidal rivers and shelf) without the erection of coastal constructions. A comprehensive comparison to in-situ measurements and remote sensing data demonstrated that the model is capable of qualitatively simulating sediment dynamics on the subaqueous delta. Another study by Le Xuan et al. (2019) investigated sediment dynamics and morphodynamic changes in the Mekong estuaries and coastal zone, using a well-calibrated Delft3D model for simulations of the coastline without the presence of offshore breakwaters. Investigations pointed out that the influences of upstream sediment reduction and large-scale sand extraction would cause substantial modifications in the subaqueous

delta region. Modeling results also showed that the sediment volume and spatial distribution changed through the simulated period according to monsoonal variation. Thanh et al. (2021) focused on modeling the entire system with a process-based approach with Delft3D and Delft3D Flexible Mesh (DFM). The first model was used to detect the sediment dynamics in coastal areas, and the second model was used to allow easy coupling between 1D and 2D grids for analyzing complex river networks. However, the study did not include offshore breakwaters in the investigations of wave reduction and sediment dynamics. The verification results show that the amount of sediment received is much lower than estimated. Vinh et al. (2016) also simulated numerically using the Delft3D model and found that the sediments mostly settled in the estuary and close to the mouths under calm conditions. Also, the higher suspended sediment levels expand offshore with higher waves conditions. In addition, a number of inland sediment transport studies in the Mekong Delta have been carried out by Manh et al. (2014), Ogston et al. (2017) and Xing et al. (2017). Heege et al. (2014), Meselhe et al. (2017) and Anthony et al. (2017) all used remote sensing to study sediment dynamics in the Mekong Delta however this remote sensing data can only explain past sediment dynamics.

Le Xuan et al. (2020, 2022) investigated the effect of incident waves and breakwater's porosity on the capacity of wave transmission, reflection, and wave energy dissipation with fixed bed morphology. Neither of those studies have investigated the toe erosion and bed morphological changes due to the breakwater-structure interaction. Based on our literature review there are no previous studies that have used laboratory physical and numerical models for VMD to understand the important role of offshore breakwaters play in terms of coastal erosion, alteration, and bed morphological changes. This is largely due to the fact that large-scale 2D/3D numerical simulations are typically unable to describe in detail offshore breakwater structures as well as

accurately determine the sediment transport rate through the structure due to the complexity of the breakwater geometry and wave-structure interaction mechanisms. This challenge can be solved by the parameterization of sediment transport rate and wave transmission processes for numerical simulation on a large scale. Alternatively, a 3D model could be applied to simulate the wave-structure interaction and sediment transport through the offshore breakwaters, however this would be very expensive and time consuming and also unable to reproduce results on a very large scale.

The objective of this study was to use a physical model to experiment the toe erosion and morphological changes caused by breakwaters in the oceanographic environment of the VMD. Three breakwaters designs that have been widely applied in the VMD were investigated:

- Pile-rock breakwaters (PRBW) (see application in the VMD in Le Xuan et al. 2020)
- Hollow Triangle Breakwaters (HTB) (see application in the VMD in Le Xuan et al. 2022),
- Semi-circular breakwaters (SBW) (see application in the VMD in Tran et al., 2018)

To achieve this objective laboratory analysis was used as a basis to understand changes in morphology for larger scale simulation by parameterization. The toe erosion and accretion process were tested in a wave flume by different structural shapes of the three breakwaters.

This paper is structured as follows. In Section 2 we describe the laboratory experiments. In Section 3 we present the results and discussion. We finish in Section 4 with conclusions based on the outcome of the laboratory experiments.

2. Methodology

The laboratory experiments were conducted by using 2D physical model to mimic the actual conditions of the three breakwater structures investigated: Pile-rock breakwaters (PRBW), Hollow Triangle Breakwaters (HTB), and semi-circular breakwater (SBW) (Le Xuan et al., 2020; 2022). The wave parameters (wave height and period) using JONSWAP spectrum were obtained from the real condition of Mekong coast. The actual dimensions of three breakwaters were collected from construction drawings. The initial geometry by filling fine sand into wave flume assumes under balance condition without erosion/deposition.

2.1. Model setup

The laboratory experiments were conducted in the River and Marine Hydrodynamic Laboratory of the Southern Institute of Water Resources Research (SIWRR) from January to March 2022 (Figure 1a). The hydraulic laboratory equipment was provided and installed by HR Wallingford. The dimensions of the wave flume were a length of 35 m, a width of 1.2 m, and a height of 1.5 m. The wave generator system is equipped with an automated system of Active Reflection Compensation, which can generate irregular and regular waves with a height of up to 0.40 m and a peak period of 3.0 s. The waves are measured by the system with frequency 50Hz (accuracy ±0.1 mm).

In this experiment, a wave-absorbing roof was arranged at the end of the wave flume, using aluminum slag material placed in an iron cage with a roof slope of 1/5 (see Figure 1b). Testing of the wave absorber and working capacity of the absorbing roof were implemented before running experiments. In all test cases (i.e. different water levels, wave parameters, etc.), the test results of reflected wave coefficient from the absorbed roof are less than 10%.

Figure 1. Wave flume (a) and rear wave absorber (b) at River and Marine Hydrodynamic Laboratory, SIWWR

The model scale was chosen using a model ratio based on wave flume capacity and boundary conditions (i.e. waves, flows). A bigger ratio ensures a higher reliability of experimental results but is associated with larger capital costs for experimental setup. Based on the constraints of the flume at the SIWWR laboratory we followed a trial-and-error process to ensure that the condition is similar to Froude and the flow in the flume must be turbulent ([Re] > 10^4) (Hughes, 1993).

Table 1. Wave flume capacity and model scale calculation

Parameter	Input boundary conditions (1)	Wave flume capacity (2)	(1)/(2)	Length ratio λ_l
Maximum water level at construction (m)	2.0	≤ 0.6	2.0/0.6	≥ 3.33
Minimum water level (m)	1.4	≥ 0.2	1.4/0.2	≤ 7
Maximum wave height (m)	1.5	≤ 0.35	1.5/0.35	≥ 4.3
Maximum wave cycle (s)	5	≤ 3.0	5/3	≥ 1.7
Construction height (m)	3.0	≤ 0.6	3.0/0.6	≥ 5

Based on the computed results in Table 1, the ratio of the selected model is as follows: N_L=7 (long scale, high scale), $N_t = \sqrt{N_L} = 2.65$ (time scale), $N_v = \sqrt{N_L} = 2.65$ (velocity ratio), and $N_m = N^3_L = 343$ (mass ratio).

In the process of analysis and selection of scale, the model size must be similar in terms of Froude number: $F = \frac{V}{\sqrt{gL}}$ (V is wave velocity; L is pore diameter). The selection according to the dimensional analysis and Buckingham's law Π helps the model to guarantee the Froude similarity index. i.e. $F_m = F_n$ (m: model; n: prototype)

The dimensions of rock with diameter D to build the PRBW construction in the experiment must ensure turbulent conditions ([Re] > 10^4) for flow through the rock layer. These conditions of flow though the rock layer were checked using formula (1).

$$Re = \frac{\rho v D}{\varepsilon \mu} \quad (1)$$

Where v is the velocity of the wave flowing through the pores, D is the diameter of the rock, μ is the absolute viscosity of the liquid (0.001002 Kg/ms), ε is the porosity of the rock layer used for the experiment (ε=0,4). The calculation results show that in the extreme case with the smallest experimental rock diameter, the smallest wave velocity, the Reynolds number Re = 20,559 (Re > [Re]) ensures the flow through the layer is turbulent.

For sediment transport, it is assumed that the fine sediment transport through construction is dominated by waves action and the predominant mode of movement is suspended transport. Ire & Nadaoka. (1984) conducted an experiment of sediment transport in front of a vertical breakwater and established the following criteria for the sand to be in suspension: $U_w/W_s \geq 10$ where U_w is the velocity of bottom particle, and W_s is the settling velocity of particle. Oumeraci (1994a) argues that the ratio of Froude numbers should be guaranteed for all hydrodynamic processes but sediment characterization should be ensured as the predominant transportation. The settling velocity of particles W_s is a key parameter to determine the mode of sediment transportation because it combines the properties of density, size, shape and viscosity. According to Oumeraci (1994a), the model scale of the settling velocity N_w should be selected according to the velocity ratio of the Froude coefficient i.e. $N_w=N_L^{1/2}$. The settling velocity was calculated according to the equation (2) (Soulby et al., 1997).

$$w_s = \frac{\nu}{d}\left[(10.36^2 + 1.049D_*^3)^{1/2} - 10.36\right] \quad (2)$$

Where $D_* = \left[\frac{g(s-1)}{\nu^2}\right]^{1/3} d$; ν is the kinematic viscosity coefficient, d is the particle diameter, g is the gravity acceleration, $s = \frac{\rho_s}{\rho}$ is the relative density where ρ_s is the density of the sediment and ρ is the density of water.

The bottom sand grain size is mainly 200 micrometers in diameter and the settling velocity is greater than 0.1 m/s as obtained from the Lower Mekong Delta Coastal Zone (LMDCZ) project (SIWRR, 2018). Quartz sand with a grain diameter d_{50}=80 micrometer was used as it is generally found in Vietnam is the best fits the model ratio of the settling velocity.

To ensure similarity with the actual conditions of coastal topography, wave shoaling and wave breaking features in Mekong Delta from deep to shallow water area, we created transitional base with a slope of 1/25 located at a distance of 5 meters from the wave generator in the wave flume. The front and back basins were filled with a 10cm thick layer of fine sand (yellow color) extending from the top of the transition slope to the foot of wave-absorbing roof (Figure 2).

Seven wave gauges were set up in front of and behind the breakwater construction including five gauges (WG1, WG2, WG3, WG4, WG5) measuring waves in front of the construction and two gauges (WG6, WG7) determining the wave height behind the construction (Zelt & Skjelbreia, 1992). Among them, WG1, WG2, WG3, and WG4 are arranged to measure reflection waves and input waves based on the least square method (Mansard & Funke, 1980). Furthermore, two E40 flow and velocity gauges were installed in the same location as WG5 and WG6 to validate the wave reflection caused by the construction and the absorbing roof. The cross-shore energy fluxes analysis method was employed to verify the wave reflection efficiency. In addition, the arrangement of the E40 gauges in these locations also helps with observations of flow characteristics around the breakwater construction.

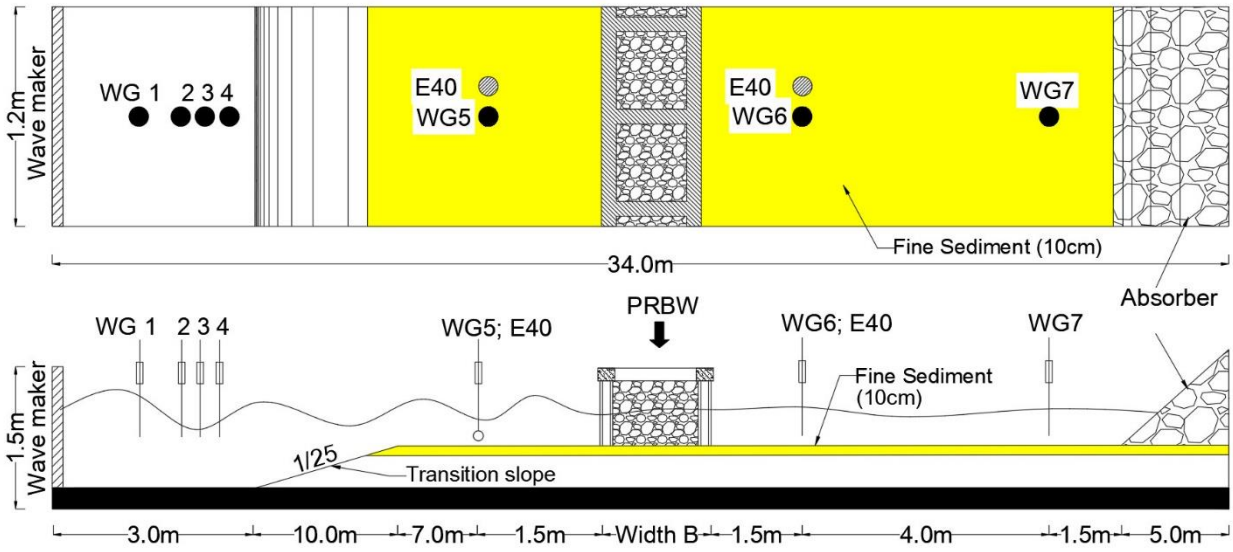

Figure 2. Example layout for the PRBW experimental setup. Note: i) the same layout was used for the HTB and SBW experimental setups, ii) the dimensions are not scale.

2.2. The three breakwaters used for the experiment

Three breakwaters design that have been widely applied in the VMD were evaluated: a Pile-rock breakwater (PRBW), a Hollow triangle breakwater (HTB), and Semi-Circular Breakwater (SBW). The actual dimensions of three breakwaters were collected from construction drawings and were downscaled to 1/7 for the laboratory experiments (Figure 3). The initial geometry by filling fine sand into wave flume assumes balanced conditions without erosion/deposition occuring. The model dimensions of three offshore breakwaters are described in detail in Table 2. To ensure that the three breakwaters were able to work under an emerged state to neglect the sediment transport in overtopping process, we setup the same water depth D=25cm (R_c=15cm) across the experiments. Due to real design of three breakwaters, the porosity of the PRBW is 40% while the percentages of front side perforation for HTB and SBW are 17.1% and 12.3%, respectively. The percentages of back side perforation for the HTB and the SBW are 12.4%

and 5.5%, respectively (Table 2). A detail description of these three breakwaters can be found in Le Xuan et al. (2020, 2022).

Table 2. Specifications of three breakwater for the experiment

Parameter	Pile-Rock breakwater (PRBW)	Hollow triangle breakwater (HTB)	Semi-Circular breakwater (SBW)
Construction height (h, cm)	40	40	40
Porosity (P, %)	40	- $P_{front\ side}$ = 17.1 - $P_{back\ side}$ = 12.4	- $P_{front\ side}$ = 12.3 - $P_{back\ side}$ = 5.5
Width (B, cm)	38	B_{bottom} = 34.4; B_{top} = 7.7	Diameter d= 64

Figure 3. Three structures for the laboratory wave flume experiments (a) pile-rock breakwater (PRBW), (b) hollow triangle breakwater (HTB) and (c) semi-circular breakwater (SBW).

2.3. Materials used and bed morphology observation method

The sand particles of mean particle diameter ranging from, d=0.2 mm to d=0.08 mm is engaged to simulate the bed morphological change and toe erosion behavior of the breakwaters in the deltaic coast having sand-mud sediment formation. The sediment formation and distribution of the wave flume are decided based upon the three primary assumptions as described as follows:

1. The Mekong deltaic coast is mostly governed by sand-mud sediment formation. The coastal erosion process is taking place strongly in recent decades, whereas in many areas of mangroves have disappeared, which refers that the fine-grained sediments from the mangroves area have been pulled away, and sand has invaded many places from the offshore coasts, resulting in a formation of a mixed formation of sand and mud. In 1973 the total mangrove area of an estimated 185,800 ha, is decreased to 102,160 ha in 2020 as shown in Figure A1 (Phan et al. 2015; Phan and Stive, 2022). There are lots of changes in sediment formation and distribution continue over the recent decades particularly the fine sand and fine silts are now the dominant sediment form.

2. This study initially carried the field measurement and observation to investigate the responsible factors of morphological change and toe erosion. The sediment distribution was considered from the field measurement by Lower Mekong Delta Coastal Zone (LMDCZ-AFD) project in 2018. The field observation is taking place at the constructions in Ca Mau, on the west coast of the Mekong Delta. Sampling results of bottom layer sediments along the coastal zone of the Mekong Delta showed that two types of sediments are dominated: fine sand and fine mud (Figure A2). The particle size distribution in the coastal area of the Mekong Delta demonstrates

that fine sand and fine silt are the dominant forms of sediments in this coastline that facilitate the mangrove plants in recent years (Figures A1 and A2). Some pictures were taken at the site of the forest area to show the fine sand and fine mud distribution on the East coast (see Figure A3). However, from our field investigation most important finding was that sand erosion which is the dominant reason for breakwaters' toe instability. Field tests conducted after construction reveal that the structures often have good wave-damping effectiveness and, in areas with abundant alongshore sediment supply, the primary reasons for breakwaters instability were caused due to sand accretion rather than mud.

3. High wave dissipation by the breakwaters results in a negligible amount of mud accretion around the structure and, as a result, very little mud accumulation happens. Therefore, in experimental testing for breakwater stability analysis of the Mekong delta, the breakwaters are frequently encouraged to engage in the formation of sand bed rather than the mud bed formation (Tuan et al. 2022). Other reasons are the experimental test of mud transport alone is complicated due to the flocculation and re-suspension phenomena. In addition to following physical laws such as advection and diffusion, mud particles are also governed by chemical and biogeochemical processes. The muddy bed formation also results in high turbidity of the water, which makes difficult to take instantaneous measurements of the bed morphology by the camera sensors. Therefore, we have used quartz sand as fine sediment in maintaining proper sediment distribution to conduct the experiment.

The experimental topography of the bed in the wave flume was flattened before the experiment and was calibrated with an SW50M laser ruler (accuracy ±1/100mm). All morphological changes around the construction were recorded using a high-speed camera placed perpendicular to the wave flume and in a fixed location over the duration of the experiment. This helps increase the accuracy

of images digitalization and extraction of morphological evolution that are captured from cameras. The camera viewport was set up to observe the change of morphology within a window of +/- 1.5m around the construction. After every hour, the wave paddle from the wave generator was temporarily stopped to measure the morphological change and toe erosion and then the experiment was continued running after the measurement was finished. The time-lapse imaging technique was applied to capture high resolution images for bed evolution analysis. The Grapher software was used to define the coordinates of every single point from contiguous surface between quartz sand bed level and water volume. The validation process was conducted to verify the digitization of bed level changes by comparing with results of laser ruler measurement.

2.4. Experimental scenarios

The input wave parameters are selected from measured data and simulation results from the numerical modelling (MIKE21-SW), in which the typical wave parameters for the Mekong Delta have wave height of 0.5m to 1.5m and a wave period from 3s to 7s. The wave parameters (wave height and period) using JONSWAP spectrum were obtained from the real conditions on Mekong coast. In the wave flume with model scale NL=1/7, wave height is ensured to greater or equal to 5cm and not higher than 30cm. The minimum wave period was greater than or equal to 1s and no longer than 3s. Irregular waves that have characteristics of deep-water waves with H_s=17 cm, wave period T_p=1.89s (equivalent to field observation: H_s=1.2m; T_p= 5.0s) were selected for the experiment.

In general, these breakwater constructions mostly work in the field in the emerged state with a positive relative freeboard (R_c>0). Therefore, this study focuses on experiments of morphological

change and toe erosion when the construction works in an emerged state with relative freeboard R_c=15cm (equivalent to 1.05m in the field).

The data obtained from each experiment for each breakwater used for the analysis was performed over a period of 15,000*T_p(s) (8 experimental hours). The time length was varied for different types of toe erosion. For example, foot erosion occurring on the vertical wall of the breakwater can reach steady state after 3000 waves for small to medium sized rocks while around 10,000 waves are required for a sand beach (Powell & Whitehouse, 1998). Therefore, as the mud-coast of the Mekong delta has fewer sand attributes, we tested for 3000 irregular waves per one experiment. Finally, the frequency range of the generated wave was clipped and taken between 0.01Hz and 1.5Hz with a calculated interval of 0.01 s/value.

3. Model results

3.1.Changes in wave spectrum through the three breakwaters

To understand the changes to the wave spectrum through the three breakwaters we need to first consider the way that the waves move through the laboratory flume. The waves were generated using wave generators in deep-water boundary conditions. Then, as the waves propagate through the flume onto the transitional base, the waves break changing the wave height and period — this is due to the influence of the reduced water depth and the so-called wave shoaling phenomenon. After the waves break, they continue to propagate into the shallow water in front of breakwater construction. The wave-breakwater interaction occurs in the form of reflected and transmitted waves.

The change in wave characteristics through the transition floor of the flume is shown using variance density spectrum of the wave energy spectrum (see WG1 in Figure 4a). The wave peak

significantly attenuates after passing the transition zone, causing significant decreases in the energy peak (see WG5 in Figure 4b). The wave spectrum has a sharp peak at deep water area (WG1 position), then much more flattened shape and more peaks after passing through transitional floor of the flume (WG5 position).

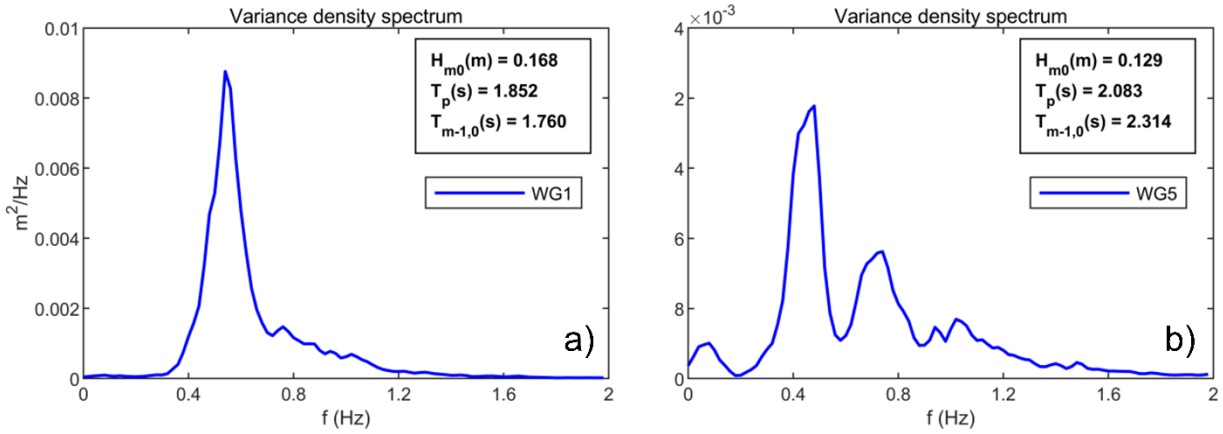

Figure 4. The variability of wave spectrum through the transition area in the wave flume from a) WG1 to b) WG5

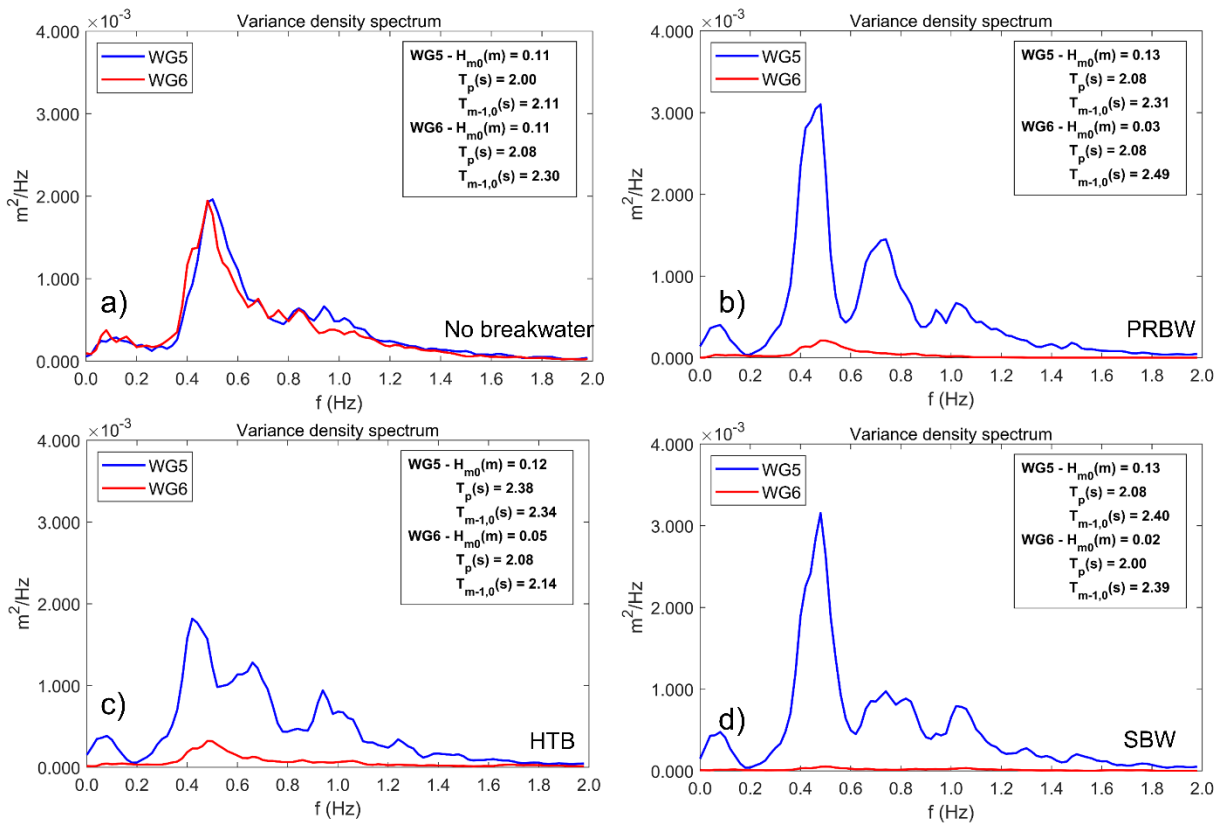

Figure 5. Variation of wave spectrum in front of (WG5) and behind (WG6) breakwaters for transmitted waves under four conditions: a) No breakwater (TH0), b) Pile-rock breakwater (PRBW), c) Hollow triangle breakwater (HTB), and d) Semi-circular breakwater (SBW).

The wave-structure interaction also varied with the three different shapes of breakwater as shown in front of the breakwater (WG5) and behind the breakwaters (WG6) in Figure 5. These results indicate the energy spectrum after passing through the breakwater structure due to wave reflection, wave transmission and wave dissipation processes. The variance density spectrum behind the breakwater (WG6) almost flattened for the SBW, while the HTB shows a relatively higher variance density spectrum than the SBW. At the same conditions of input waves, water depth, topography, the SBW has the lowest transmitted wave height (Figure 5d). Among the three breakwaters, the

HTB has the highest transmitted wave energy of 3.2×10^{-4} (m^2/Hz) (Figure 5b) and followed by the PRBW by 2.2×10^{-4} (m^2/Hz) and the lowest attributed to the SBW with 0.51×10^{-4} (m^2/Hz).

The differences in the reflected wave spectrum for the three breakwaters is shown in Figure 6. Accordingly, the PRBW structure has the largest reflected wave energy of 5.0×10^{-4} (m^2/Hz) as it is a permeable vertical wall, while the HTB and SBW structures both have similar spectra of reflected waves of 2.28×10^{-4} (m^2/Hz) and 2.52×10^{-4} (m^2/Hz), respectively due to the similarity of their shape, peak energy, and frequency distribution (Figure 6b, c). The wave energy dissipation of the SBW is higher than those of two other breakwaters. On the other hand, the PRBW has lowest wave energy dissipation compared to the other two breakwaters.

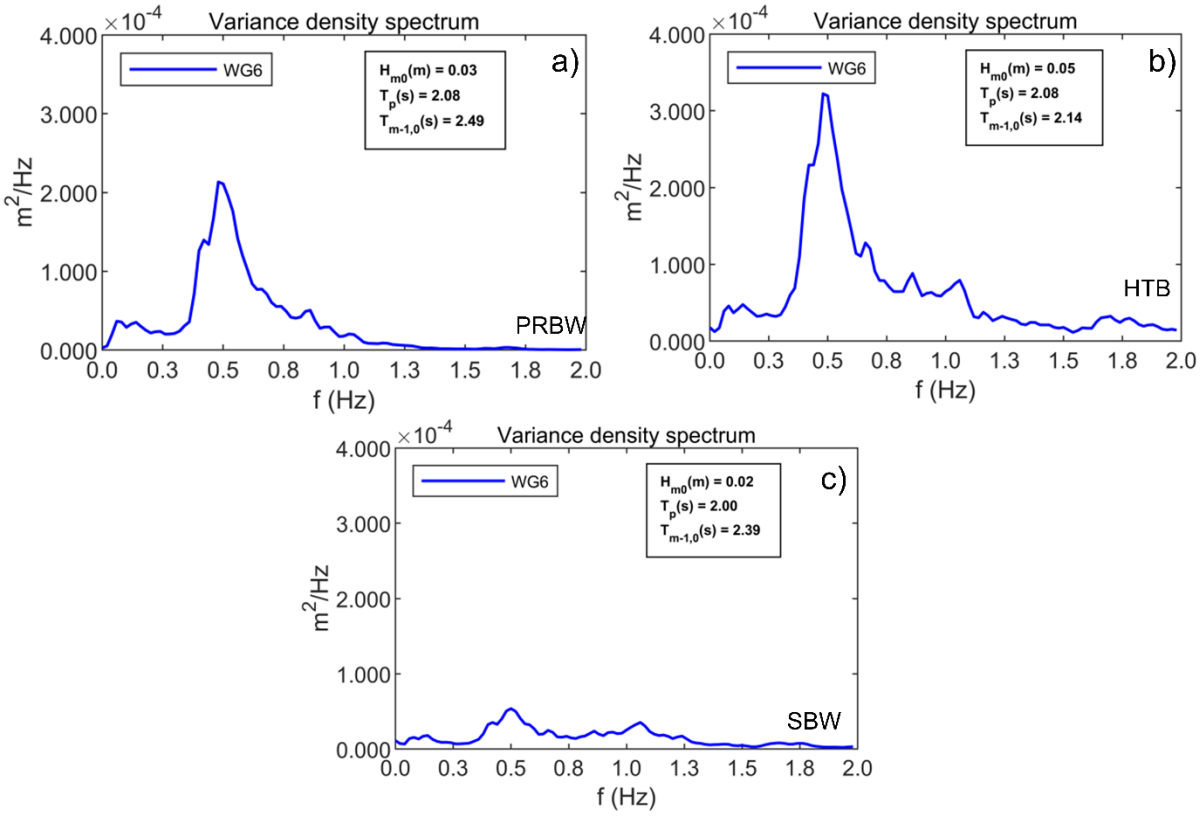

Figure 6. Reflected wave spectrum for the three breakwaters. a) pile-rock breakwater (PRBW), (b) hollow triangle breakwater (HTB) and (c) semi-circular breakwater (SBW)

3.2. Variability of wave patterns through the three breakwaters

To understand the changes to the direction, magnitude, and frequency of waves through the three breakwaters we considered the wave-induced currents patterns at two positions: in front of the breakwater (WG5 and E40 as shown in Figure 2) and behind the breakwater construction (WG6 and E40). The results of wave-induced currents in front of the breakwater are presented in Figure 7 and the results for behind the breakwater are presented in Figure 8. In each case we consider four cases a) no breakwater (HT0), b) presence of PRBW, c) presence of HTB, and d) presence of SBW.

Figure 7 shows the front currents of the three breakwaters have larger values at WG5 than in the case of no breakwater. The current after the structure are higher speed and longer frequency, which facilitates the transportation of sedimentation to the shore. The current characteristics in Figure 8 show there is significant decrease of current speed behind the construction due to the presence of the breakwater structures. Among the studied breakwaters, the SBW has the highest wave energy dissipation efficiency, and so it is expected that it has the lowest wave-induced current speed in comparison to the other breakwaters (Figure 8d). The PRBW has medium wave energy dissipation efficiency and has performance in between the other two other breakwaters ((Figure 8b). The HTB has the highest current speed behind the construction as it has the lowest wave energy dissipation efficiency (Figure 8c). These results indicate that the shape of the breakwater significantly influences the current speed. The wave current speed behind the breakwater is dependent on the breakwater shape and structure and higher wave current speeds may cause high erosion resulting in long-term breakwater instability.

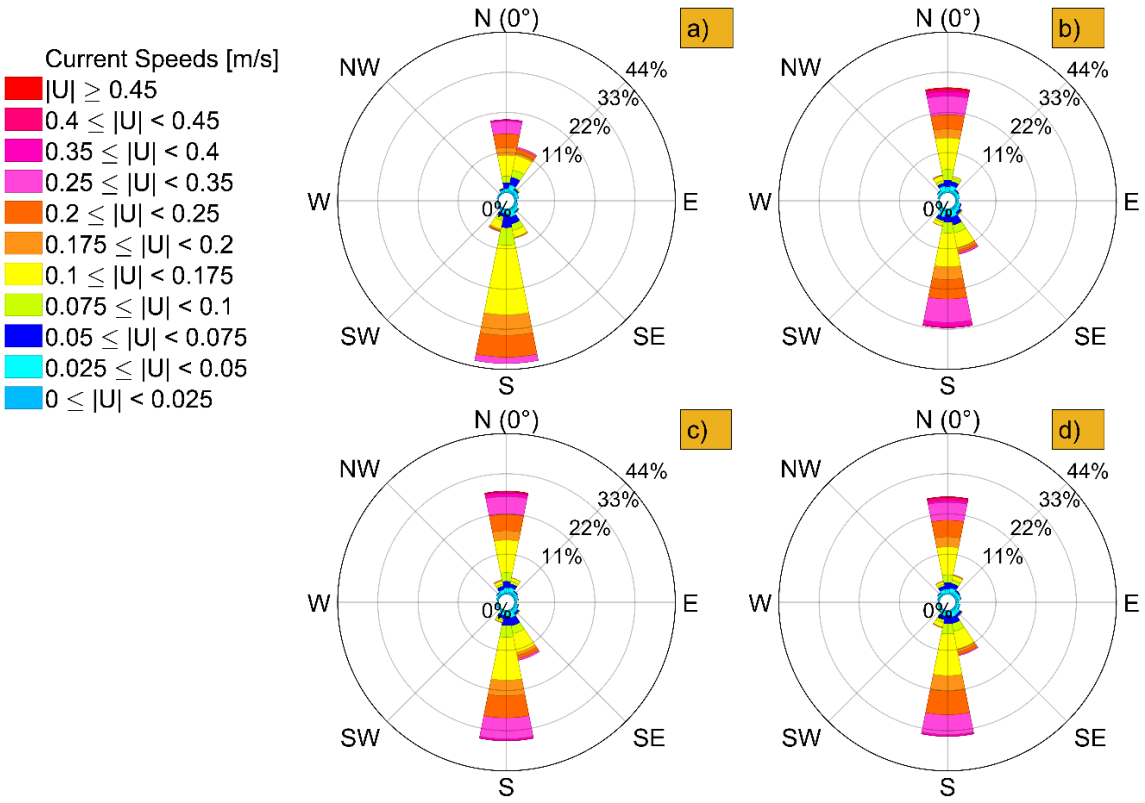

Figure 7. Current rose in front of three breakwaters (WG5). a) No breakwater (TH0); b) pile-rock breakwater (PRBW); c) hollow triangle breakwater (HTB); d) Semi-circular breakwater (SBW)

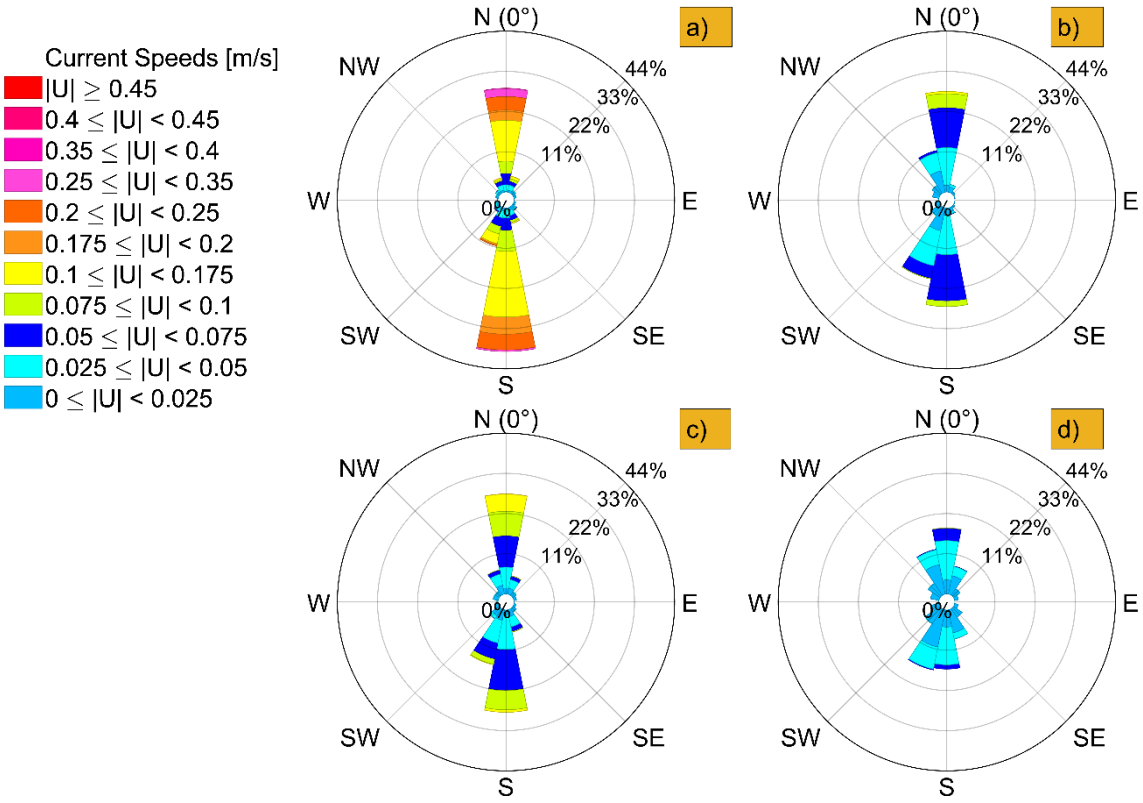

435

436 Figure 8. Current rose behind three breakwaters (WG6). a) No breakwater (TH0); b)

437 pile-rock breakwater (PRBW); c) hollow triangle breakwater (HTB); d) Semi-circular

438 breakwater (SBW)

439 ***3.3. Changes of bed morphology surrounding the three breakwaters***

440 To understand the changes to the bed morphology surrounding the three breakwaters we examine

441 the annotated results in Figure 9 which indicate the erosion in front of the pile-rock breakwater

442 over time. We investigate the erosion holes in the bed of the wave flume to get an idea of the

443 magnitude of consequences associated with setting up the different types of breakwaters.

444 Specifically, over an experiment run of 8 hours the PRBW produces erosion holes 50cm wide

445 approximately 7.5cm deep in front of the breakwater structure (Figure 10 – top panel). Behind the

446 breakwater small erosion holes also developed, 10cm away from toe of the construction on the

direction of absorbing roof. The depth of the erosion holes in the mudflat varies from 4cm to 7.5cm depending on the experiment run time (Figure 10 – bottom panel).

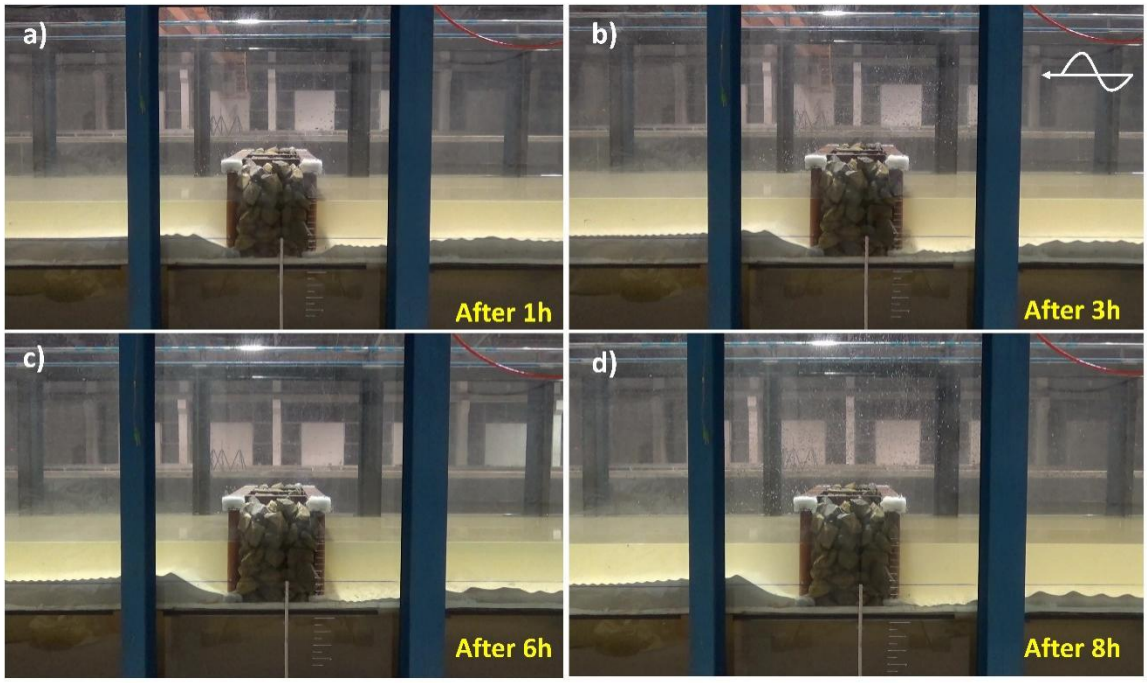

Figure 9. Morphological change of beach over the time for PRBW

Figure 10. Picture of erosion in front of and accretion behind the PRBW

Change in bed morphology around the HTB structure and the SBW structure have similar patterns to the PRBW. In each case, the depth of the erosion holes in front of the breakwater increased with experiment run time. Looking specifically at the HTB in Figure 11, while the mudflats appear flat, there are erosion holes at the toe of the breakwater construction, as well as behind the construction. Examining the HTB and SBW in in Figure 12 we see that front of the SBW breakwater some local erosion holes were observed but the height of accumulated sediment deposits behind the construction were smaller than in the case of the HTB structure. The accumulated sediment deposit or mudflats behind the HTB was observed to be 67cm in length and on an average 5cm in height.

We further examine the changes in bed morphology around the SBW in

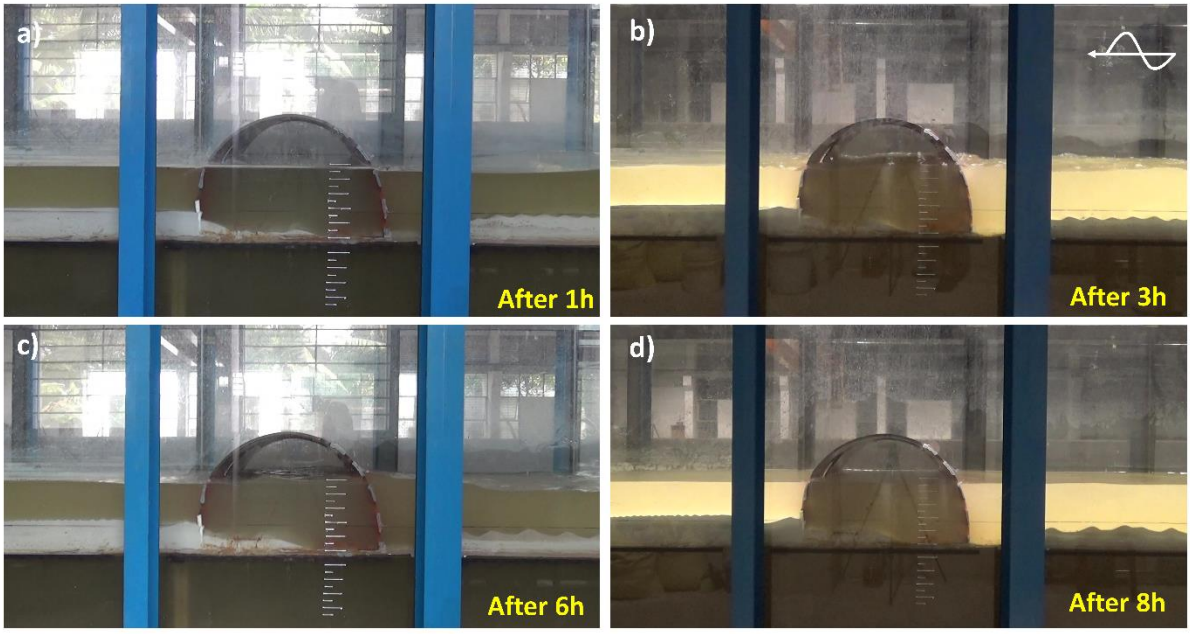

Figure 13. In the front section we see erosion holes with dimensions 30cm in length and 9cm in depth. Nevertheless, the toe of SBW construction was less eroded than the other two classes of breakwaters. The mudflats formed by sediment deposition also has a much smaller volume in the case of the SBW. In

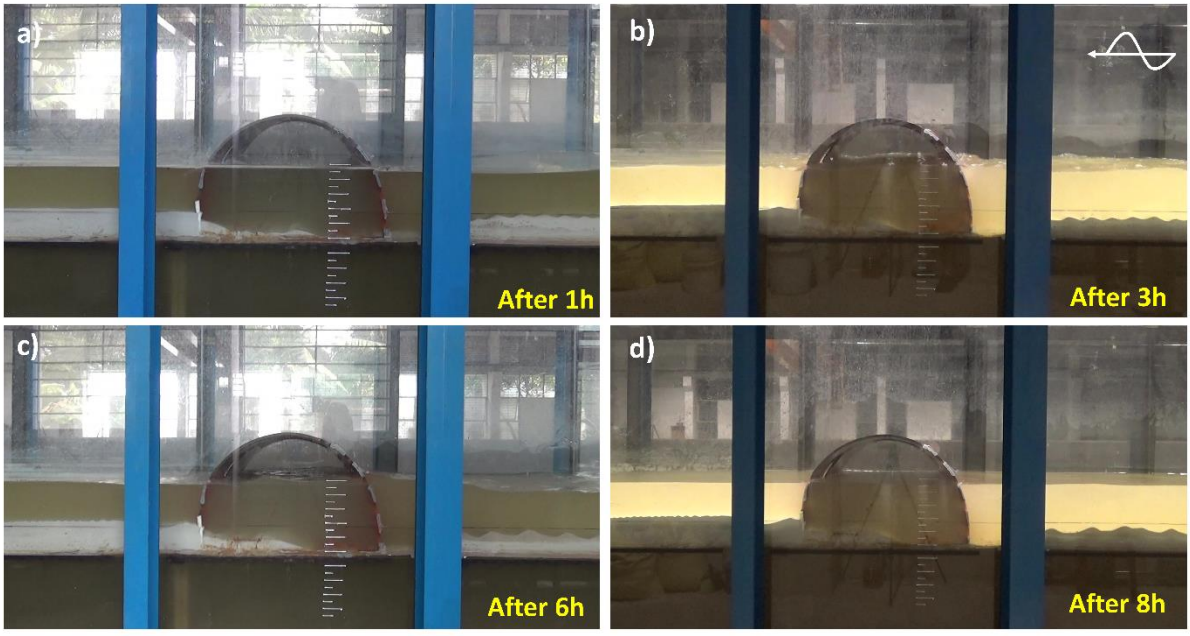

Figure 13 we see 2cm-3cm high mudflats. One advantage of forming mudflats behind the breakwater is that it contributes to lateral stability that helps to resist the wave force. However, the depth of toe erosion observed is most concerning because it may result in breakwater failure.

Breakwater instability can be managed by improving the design of the berm at the toe or by reinforcing the construction with stones on the front and back feet of the construction. Traditional breakwaters may require berms at the toe to decrease bottom settlements and limit scour holes in front of the barrier caused by coastal currents. In the meantime, they may be more successful than straight-sloped conventional breakwaters without a berm at increasing the armor layer's stability and reducing the wave overtopping discharge (Celli et al. 2019). Berms at the toe of the breakwater have a range of benefits including reducing the wave load on the breakwater, reducing settlement of the breakwater in beach sites or in cases of poor soil, reduce wave overtopping discharge, and decrease the liquefaction probability (Celli et al. 2018). One major problem, setting up the breakwater without a berm is the requirement of frequent maintenance. On the other hand, setting up a berm for the breakwater in some cases restricts the sediment exchange on the leeside of the breakwater which plays a considerable role in restoring the mudflat for mangroves in the deltaic coast (Tran et al, 2018; Le Xuan et al. 2022). In deltaic coast such as the Vietnamese Mekong delta the environmental exchange through breakwaters plays a significant role in restoring the mangrove forest. Besides that, the ecosystem of the mangroves requires critical support from regular tides (Albers & Schmitt, 2015; Winterwerp et al., 2020).

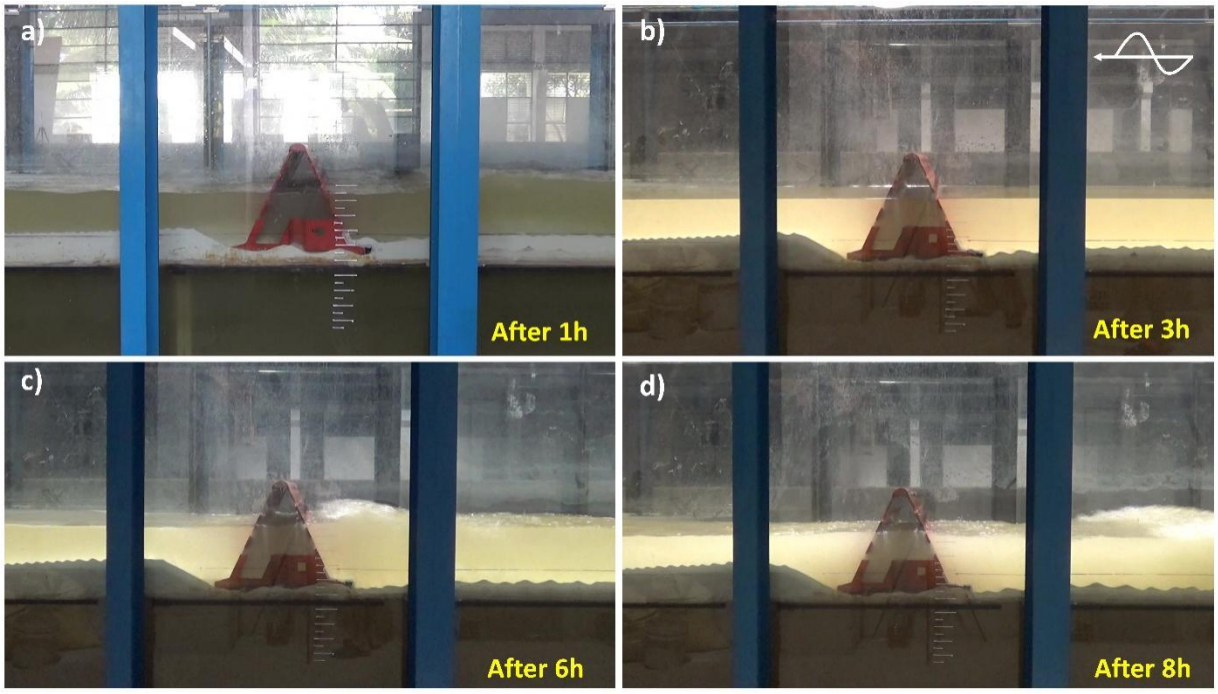

Figure 11. Morphological change of beach over the time for the HTB

Figure 12. Toe erosion at HTB and SBW, in front of breakwaters (left panel), accretion behind the breakwaters (right panel).

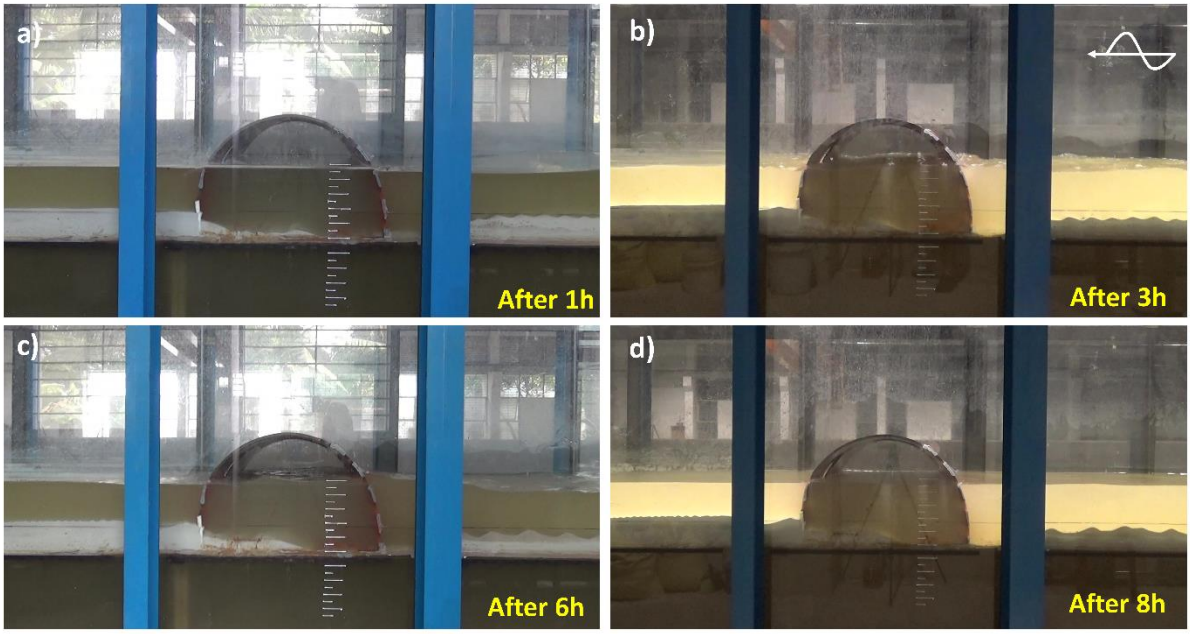

Figure 13. Morphological change of beach over the time for SBW

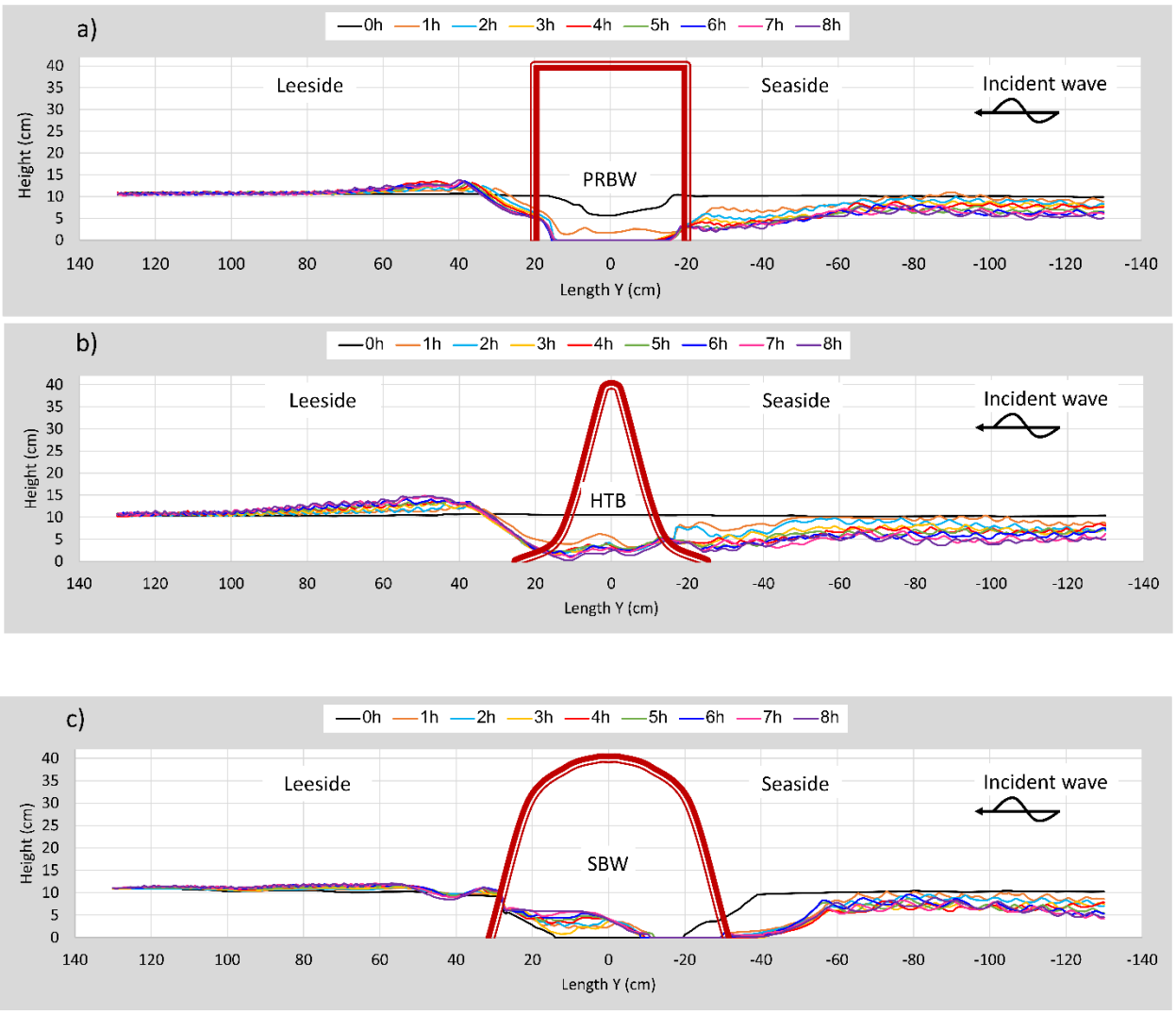

Figure 14. Morphological evolution of beach due to wave-structures interaction at different time measurements over the experimental period of 8 hours.

We investigate the changing bed morphology over time with different breakwaters in Figure 14. The bed morphology in front of the PRBW structure shows the scour hole depth reaches 5-7 cm over time. The seaside scour holes in the case of the PRBW are larger than the other two breakwater types. The scour holes for the SBW structure occur at certain distances (40-50 cm) from the seaside toe in front of the breakwater. As the experimental run time increases, we observe

505 a significant amount of sediment trapped inside the hollow body of the SBW (Figure 14c). The
506 bed morphology of the HTB structure shows the erosion depth at the leeside toe is higher than the
507 seaside toe (Figure 14b). We also see that the permeability of the breakwater has significant
508 influence on wave current dissipation. The hollow breakwater shapes help to dissipate wave
509 currents. This can be explained by the effect of the structure's permeability in reducing the wave
510 reflection properties as well (Oumeraci, 1994b; Le Xuan et al., 2020). However, the circular shape
511 can increase the vertical component of wave current in the toe region which is responsible for the
512 scour hole formed on the seaside of the breakwater (Neves et al. 2007; Dhinakaran, 2011; Huang
513 et al. 2011).

514 The increase in erosion in front of SBW also depends on the arrangement of the near bottom holes
515 in the SBW design. Flow through the near bottom holes is narrow which leads to an increase in
516 velocity and sediment near the bed which could wash towards the leeside. Otherwise, the back side
517 of the SBW is relatively closed with two rows of holes arranged in the middle of arc that block the
518 transportation of sediment to the leeside.

519

520 ***3.4. Erosion and accretion rate areas on seaside and leeside of the three breakwaters***

521 It is well-known that the wave characteristics (wave height and period) will change when
522 waves go through a shallow water area. The reciprocal interaction between waves and topography
523 lead to changes in wave characteristics and also consequently bed morphological changes and vice
524 versa. This was clearly observed during the first 1 hour of the experiment run time.

525 Take the result of the no breakwater case (TH0) as an example. The period from 0h to 1h
526 results in the most significant alteration of bed morphology (see Figure 15). The change of total
527 area in front of and behind the breakwater during 1h to 8h only fluctuates around the value at 1h

and not excess more than 5% (Figure 15a). This shows that the interaction process of waves and topography is being self-adjusted and gradually stabilized. Similarly, in the period from 0h to 1h for the case of erection of the breakwater the self-regulating process of morphological change also takes place. Especially, for hollow structures such as HTB, SBW with perforation on both faces of construction, a certain amount of sand will be pushed into the interior of the breakwater under the force of the first incoming waves. This leads to quick loss of the amount of sand at the front foot of the breakwaters. Meanwhile, the SBW has a row of holes on the bottom of the front of the structure located lower than those in HTB and the back row of holes is higher than those in the HTB. This causes the SBW to have the highest front side erosion rate the first hour (see Figure 15a).

Changes in bed morphology in terms of erosion and accretion is determined by measuring the change in annotated area in front and behind the breakwater cross-section. As explained above, the period from 0h to 1h is the self-regulating period for morphological change. So, to provide an exact view of the erosion rate of various types of breakwaters we must consider the time after 1h onwards.

The percentile change in vertical cross-sectional area were calculated using the following formula:

$$\%S = \frac{S_t - S_0}{S_0}$$

While: %S is the percentile of change

S_t is the cross-section area at time t

S_0 is the initial cross-section area

549 Looking at the results in Figure 14 we see that the erection of the breakwater not only alters
550 the wave characteristics but also changes the bed morphology and front toe erosion of construction.
551 Due to the influence of the narrow flow through the holes that creates accretion behind the structure
552 far from 30cm from the back side of the structure.

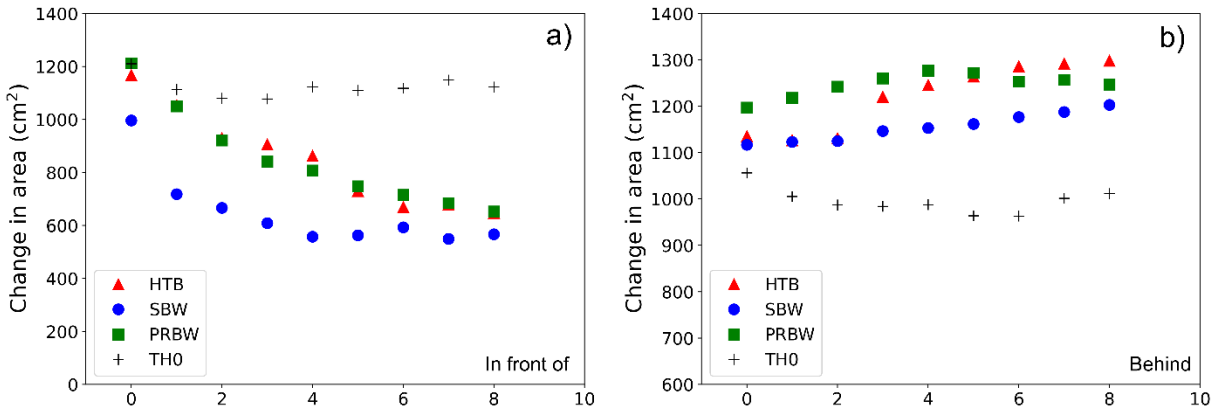

553

554 Figure 15. Changes in the vertical cross-sectional area in front of (a) and behind (b) breakwaters
555 over the time.

556 Figure 16 demonstrates the change of vertical section in front and behind the breakwater
557 over time and with breakwater types. At the front section or seaside, the fastest erosion was
558 recorded for the SBW structure, followed by the PRBW and the lowest erosion processes occurred
559 in the case of the HTB. The seaside SBW erosion reached a stable state after running the
560 experiment 4 hour. After one hour of testing, the sediments at the foreshore of the SBW structure
561 have been reduced by 30%, and this erosion rate is 15% for PRBW and 10% for the case of HTB,
562 respectively. However, after more than 5 hours of experimentation, the evolution lines of the
563 structures began to converge, showing that the stabilization process of the foreshore was similar
564 between the structures. At that stage, the percentile of eroded sedimentation is around 40%-45%.
565 The erosion process is still occurring at this point as demonstrated by the downward trend. In the
566 no construction scenario (TH0), the process line tends to be horizontal, indicating stabilization at

foreshore and backshore has occurred. However, we still observe continuous growth of small mud bars disappearing in a cyclic pattern which are negligible in the overall change of the area. The sedimentation process line is a noticeable covariant with time for the leeside of the construction as observed in Figure 16b. The accretion process leeside of the breakwater, shows the cumulative growth of mudflats over the experiment time. However, the accretion rate is much lower than the foreshore erosion rate, as indicated by the slope of the process line in Figure 16a and Figure 16b. During the eight hours of the experiment runtime, the HTB structure has the largest accumulation rate in the backshore with 15% of initial area added. The PRBW and the SBW back shores have increased by 5% and 7% of the original area after the experiment, respectively.

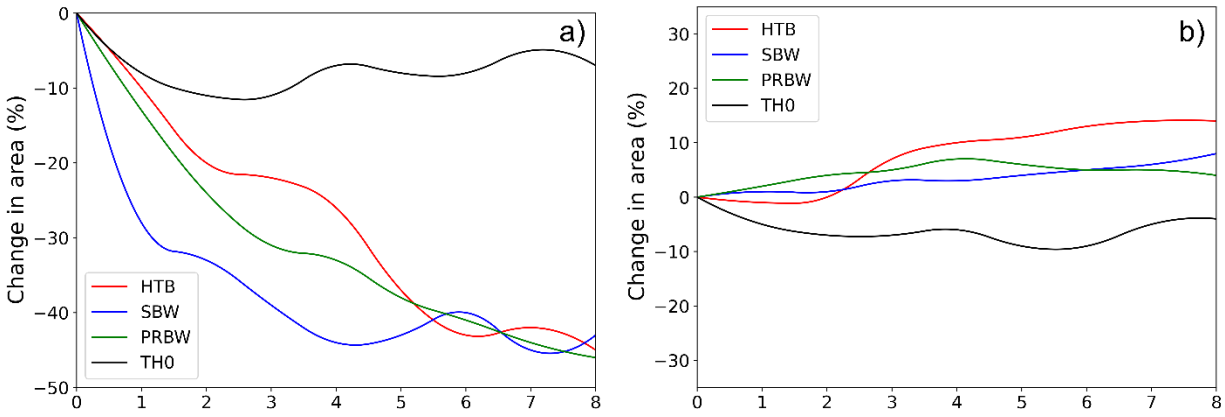

Figure 16. Percentage of change of vertical cross-section area over the time. a) in front of the breakwaters, and b) behind the breakwaters

Next, we examine the area of erosion in Figure 18. The erosion rate for the SBW in the period from 1h to 4h is also approximately equal to the erosion rate of the other two breakwaters (HTB, PRBW). The accretion rate for the SBW in the same period is lower than those for PRBW at about 2 - 3%. The bottom row of holes for the backside of the SBW in is higher than those for HTB so the fine sediment in the early stages has less capacity to pass through the structure compared to the HTB. Most of sediment volume is left inside the structure and wave dissipation

coefficient (K_d) is largest. However, during the period 5 - 8h when the erosion speed is increased there is a similar trend of variation as in the case of the no construction scenario (TH0). This shows that the fine sediment is brought away from the inside of the structure and deposited on the backward. The accretion process starts to formulate behind the structure and the accretion rate gradually increases.

Average changes in the bed cross section over time are shown in Figure 17 while wave reduction efficiency and wave coefficients are shown in Figure 18. According to Figure 17b, the SBW lost 4.4% of front section area per hour and increased 0.4% of its original area per hour at the backshore. The PRBW lost 3.8% per hour at the seaside and the accretion added up to 0.5% per hour at the leeside. Among the three breakwaters, the HTB has the lowest erosion rate with average rate at 3.4% per hour and the largest accretion rate at 1% per hour. In the case of no construction (TH0), there is only erosion occurring, which is demonstrated by the decrease of 0.9% and 0.7% per hour at the bed. Figure 17a shows the cumulative area of erosion and accretion obtained throughout the experiment. The SBW demonstrates a high amount of erosion and a low amount of deposition. The HTB erosion amount at the seaside and the deposition at the frontside are close in value.

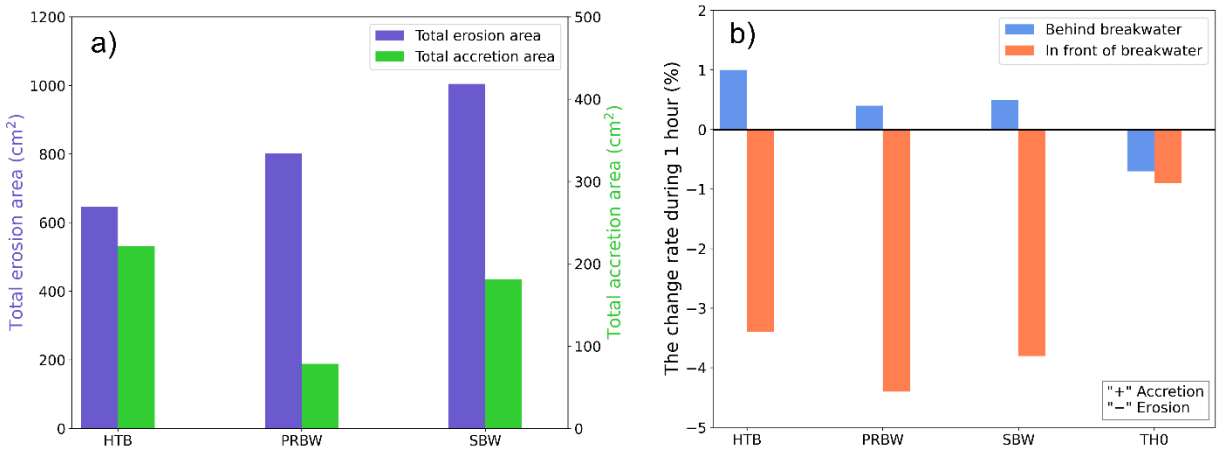

Figure 17. a) Total area of erosion in seaside and accretion in leeside and b) Average hourly changing rate of cross section.

These results show that the erosion rate in front of the HTB and the PRBW are approximately equal, but the accretion rate behind the PRBW is slower than in the case of the HTB (Figure 17b). This means that the HTB shows the ability to allow fine sediment to pass through the construction at a much higher rate than in the case of the PRBW because the wave transmission coefficient of the HTB is highest (see Figure 18). The erosion rate in front of the HTB is inversely proportional to accretion rate behind this construction. While the accretion rate behind PRBW is slower than the erosion rate in front of structure which proves that the fast front erosion rate is due to the largest reflected wave coefficient (K_r) (see Figure 18).

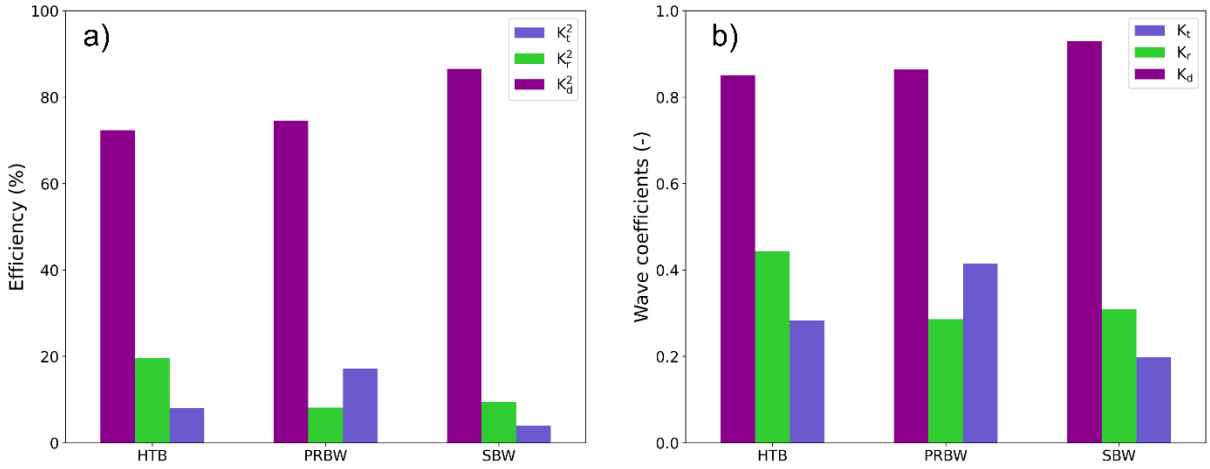

Figure 18. The wave reduction efficiency and wave coefficients for three breakwaters

4. Discussion

The design of a submerged and emerged breakwater is a very complex and subjective operation because it is founded on empirical expressions derived from experimental data. In field conditions the wave spectrum will be modified because incoming wave directions are not

619 constrained to be unidirectional as in the case as in the experiments. The oblique wave action, bed
620 morphology, soil bed properties etc. may change the toe erosion failure relationship and scour hole
621 distance (Hoby et al. 2015) for which a probabilistic optimal design can be proposed in future
622 studies. The studied breakwaters shape also indicates that the arrangement of holes and percentage
623 of perforation strongly affects the toe erosion due to reflected waves (Zanuttigh & van der Meer,
624 2008; Oumeraci, 2010; Dhinakaran, 2011). If the holes on the surface of the breakwater are too
625 close to ground, seaside toe erosion can occur at a faster rate. If the holes on the surface of
626 breakwater on the leeside are placed too high, this can limit the accretion on the leeside of the
627 construction. Finally, the arrangement of additional solutions to protect the front and rear
628 breakwater structures will help to reduce foot erosion and increase the stability of the structure.
629 This work has identified a number of key considerations for breakwater design in deltaic
630 coastlines. All three breakwater designs have advantages and disadvantages in supporting the
631 coastal protection measures in the deltaic coast. Based on the experimental results with the three
632 breakwaters considered we make the following recommendations:

633 • The HTB results in the maximum accretion amount behind the structure as well as the
634 fastest accretion rate behind the structure. Both measures are important in for mangrove
635 restoration, particularly in cases where severe coastal erosion is occurring. Therefore, we
636 recommend this type of breakwater for mangrove restoration in deltaic coastlines.

637 • The PRBW structure produced the fastest toe erosion rate in front of structure, the
638 slowest accretion rate behind the structure, and the lowest mudflat area behind the structure.
639 Therefore, we do not recommend this type of breakwater for mangrove forest restoration in deltaic
640 coast.

- The SBW structure demonstrates the highest wave reduction efficiency. Therefore, we recommend this type of breakwater in the case where there are severe wave conditions and mangrove restoration is of a lower priority.

Expensive coastal protection measures through soft and hard engineering solutions may not be feasible in many cases considering the socio-economic condition in many deltaic regions such as Bangladesh, Vietnam, India, Indonesia, and China amongst others (Winterwerp et al., 2020; Chávez et al., 2021). Further research will need to be undertaken to identify opportunities for more widespread adoption of coastal protection measures in these regions.

The field scale breakwaters require sufficient design considerations on maintaining the porosity parameter constant with time to ensure the efficiency of the breakwaters' wave energy dissipation and sediment trapping capacity. When the breakwaters are installed in the surf zone, the sediment transport could be very intensive due to wave breaking phenomena, resulting in the highly likelihood of sediment filling up inside of the breakwaters very quickly. Therefore, the hydrodynamic and sediment transport conditions of the area where the breakwaters are supposed to be placed should be observed and monitored regularly to avoid rapid porosity loss of the breakwaters. The porosity of the breakwater has a significant impact on the experimental results related to wave energy dissipation efficiency, sediment erosion/accretion around the breakwaters (Table 2), particularly when sediment is gradually filling up inside of PRBW, HTB, and SBW over time (e.g., months or years) that can subsequently reduce the porosity of the breakwaters, resulting different conclusions in field state. However, under the effect of strong wave action that hit on the breakwaters in both monsoon seasons (Northeast and Southwest monsoons) in the east and west seas, respectively, so the sediment inside the breakwaters will be eroded and wash away far from

breakwaters. The wave dynamic pushes the sediment into shoreline in the northeast monsoon due to high tide magnitude in flood season and in contrary a reverse tendency of sediment transport direction observed that pull out the sediment to the sea due to strong neap tide currents influenced by southwest monsoon. In fact, it has been reported that by Southern Institute of Water Resources Research (Le Xuan et al. 2022), the results of field measurements and observation from 2019-2021, the amount of sediment deposited inside three breakwaters is negligible because the sand transport is strongly affected by waves, tidal currents and high-water level. Moreover, three mentioned constructions are offshore and submerged breakwaters, and they are located far from the shoreline of about 150 m. Therefore, the hydrodynamic condition and wave action are very strong and the sediment decomposition inside the breakwaters can be neglected for a emerged breakwater. The experimental design of toe erosion in the mud coast needs to be investigated in future studies engaging kaolinite as a sediment form and long-term testing period because cohesive sediments take more testing period for breakwater instability than the non-cohesive sediment such as sand.

5. Conclusion

This study investigated the morphological changes and toe erosion due to wave-structure interaction for three breakwaters HTB, PRBW, and SBW. This was investigated using a 2D physical model by running 3000 irregular waves over 8 experimental hours.

The experimental results showed that the shape and structural design of breakwaters can change the bed morphology on both the seaside and the leeside of the breakwaters. The results show that the seaside, especially the toe of construction can be eroded due to reflected waves, narrow flow patterns and higher velocity due to the shape of the construction. The accretion at the leeside of the breakwater is mainly from the transported sediment through the body of construction.

Comparing the three breakwater designs, the results showed the following:

(i) The HTB design has the maximum accretion rate behind the structure and the fastest accretion rate behind the structure which is important in mangrove restoration particularly in the case of severe coastal erosion damage.

(ii) The SBW design has high wave energy dissipation, although the toe erosion rate is faster than other breakwaters. The experimental study also suggests to carefully consider to appropriately design the position of holes in both sides of the SBW breakwaters to tradeoff the erosion and accretion process.

(iii) The PRBW design also causes the accretion at the leeside of the construction, however, the accretion rate is lower than HTB.

Based on these results we recommend that practical designers give particular concern about the reinforcement of the foot of construction during designing process and stability calculation to prevent the toe erosion and increase the stability of the breakwater structures in order to ensure long-term deltaic coast sustainability. In this study, we took the extreme condition of incident wave (Hs=17 cm, wave period Tp=1.89s) to investigate the morphological change and toe erosion with long period of 15,000*Tp(s). Future research should employ the design wave conditions such as wave heights and periods with various return periods to conduct experiment testing along with various design water depths. If the experimental results of non-cohesive sediment applied to mud or mixed mud-sand coasts, the design wave heights/periods could be different as the wave heights/periods on sandy coasts are expected to be always higher/longer than silt-sand coasts. The design wave heights and water level based on sediment types should be studied before application.

The results from these experiments are critical to support the sedimentation process of deltaic coast where sediment deposition is required to maintain the coastline elevation, offset the

rapid sea level rise and long-term sustainability of ecosystem. A better understanding of toe erosion or accretion process and understanding the morphological change will help practitioners to mitigate erosion by reinforcing the foot of construction in breakwater constructions on deltaic coastlines. These findings are crucial for any deltaic coast where the sediment exchange through submerged breakwaters also play critical role for supporting mangrove forest ecosystems and ensuring the stability of sedimentation processes.

Acknowledgments

This work was supported by the Ministry of Science and Technology (MOST) Vietnam in a national project (No. ĐTĐL.CN-47/18) “Physical model experiment for investigating coastal protection measures of Mekong Delta." Many thanks to the Southern Institute of Water Resources Research for providing laboratory, equipment, and necessary information. The authors greatly appreciate the Editor and sincerely thank the two anonymous reviewers for their constructive comments to improve the manuscript.

Data Availability Statement

Datasets related to this article can be found at https://doi.org/10.17632/rsy8p5v6m2.1, an open-source online data repository hosted at Mendeley Data (Tran Anh, Duong 2022).

Declaration of Competing Interest

The authors in this paper declare no conflicts of interests.

References

Albers, T. and Schmitt, K., 2015. Dyke design, floodplain restoration and mangrove co-management as parts of an area coastal protection strategy for the mud coasts of the Mekong Delta, Vietnam. *Wetlands Ecology and Management*, *23*(6), pp.991-1004.

Anthony, E.J., Brunier, G., Besset, M., Goichot, M., Dussouillez, P. and Nguyen, V.L., 2015. Linking rapid erosion of the Mekong River delta to human activities. *Scientific reports*, *5*(1), pp.1-12.

Anthony, E.J., Dussouillez, P., Dolique, F., Besset, M., Brunier, G., Nguyen, V.L. and Goichot, M., 2017. Morphodynamics of an eroding beach and foredune in the Mekong River delta: Implications for deltaic shoreline change. *Continental Shelf Research*, *147*, pp.155-164.

Baquerizo, A., & Losada, M. A., 1999. Sediment transport around a mound breakwater: The toe erosion problem. In *Coastal Engineering 1998* (pp. 1720-1729).

Birben, A.R., Özölçer, İ.H., Karasu, S. and Kömürcü, M.İ., 2007. Investigation of the effects of offshore breakwater parameters on sediment accumulation. *Ocean Engineering*, *34*(2), pp.284-302.

Celli, D., Li, Y., Ong, M.C. and Di Risio, M., 2019. The role of submerged berms on the momentary liquefaction around conventional rubble mound breakwaters. *Applied Ocean Research*, *85*, pp.1-11.

Celli, D., Pasquali, D., De Girolamo, P. and Di Risio, M., 2018. Effects of submerged berms on the stability of conventional rubble mound breakwaters. *Coastal Engineering*, *136*, pp.16-25.

Chávez, V., Lithgow, D., Losada, M. and Silva-Casarin, R., 2021. Coastal green infrastructure to mitigate coastal squeeze. *Journal of Infrastructure Preservation and Resilience*, *2*(1), pp.1-12.

Dai, J., Wang, C.M., Utsunomiya, T. and Duan, W., 2018. Review of recent research and developments on floating breakwaters. *Ocean Engineering*, *158*, pp.132-151.

Dhinakaran, G., 2011. Hydrodynamic characteristics of semi-circular breakwaters. Sciences, 4(1), pp.1-21.

Ding, Y. and Wang, S.S., 2008. Development and application of a coastal and estuarine morphological process modeling system. *Journal of Coastal Research*, (10052), pp.127-140.

Ding, Y., Jia, Y. and Wang, S.S., 2006. Numerical modeling of morphological processes around coastal structures. In *World Environmental and Water Resource Congress 2006: Examining the Confluence of Environmental and Water Concerns* (pp. 1-10).

Du, Y., Pan, S. and Chen, Y., 2010. Modelling the effect of wave overtopping on nearshore hydrodynamics and morphodynamics around shore-parallel breakwaters. *Coastal Engineering*, *57*(9), pp.812-826.

Vinh, V.D., Ouillon, S., Van Thao, N. and Ngoc Tien, N., 2016. Numerical simulations of suspended sediment dynamics due to seasonal forcing in the Mekong coastal area. *Water*, *8*(6), p.255.

Evans, G., 2012. Deltas: the fertile dustbins of the continents. *Proceedings of the Geologists' Association*, *123*(3), pp.397-418.

Fitri, A. and Yao, L., 2019, October. The impact of parameter changes of a detached breakwater on coastal morphodynamic at cohesive shore: A simulation. In *IOP Conference Series: Earth and Environmental Science* (Vol. 365, No. 1, p. 012054). IOP Publishing.

Fitri, A., Hashim, R., Abolfathi, S. and Abdul Maulud, K.N., 2019. Dynamics of sediment transport and erosion-deposition patterns in the locality of a detached low-crested breakwater on a cohesive coast. *Water*, *11*(8), p.1721.

Giri, C., Ochieng, E., Tieszen, L.L., Zhu, Z., Singh, A., Loveland, T., Masek, J. and Duke, N., 2011. Status and distribution of mangrove forests of the world using earth observation satellite data. *Global Ecology and Biogeography*, *20*(1), pp.154-159.

Heege, T., Kiselev, V., Wettle, M. and Hung, N.N., 2014. Operational multi-sensor monitoring of turbidity for the entire Mekong Delta. *International Journal of Remote Sensing*, *35*(8), pp.2910-2926.

Hieu, P.D., Phan, V.N., Nguyen, V.T., Nguyen, T.V. and Tanaka, H., 2020. Numerical study of nearshore hydrodynamics and morphology changes behind offshore breakwaters under actions of waves using a sediment transport model coupled with the SWASH model. *Coastal Engineering Journal*, *62*(4), pp.553-565.

Hoby, P.M., Sajikumar, N. and Sumam, K.S., 2015. Probabilistic optimal design of rubble-mound breakwater. *Journal of Waterway, Port, Coastal, and Ocean Engineering*, *141*(4), p.06015002.

Huang, Z., Li, Y. and Liu, Y., 2011. Hydraulic performance and wave loadings of perforated/slotted coastal structures: A review. *Ocean Engineering*, *38*(10), pp.1031-1053.

Hughes, S.A., 1993. Physical models and laboratory techniques in coastal engineering (Vol. 7). World Scientific.

Irie, I. and Nadaoka, K., 1985. Laboratory reproduction of seabed scour in front of breakwaters. In *Coastal Engineering 1984* (pp. 1715-1731).

Klonaris, Georgios Th, Anastasios S. Metallinos, Constantine D. Memos, and Konstantina A. Galani. 2020. Experimental and numerical investigation of bed morphology in the lee of porous submerged breakwaters. *Coastal Engineering* 155: 103591.

Kondolf, G.M., Rubin, Z.K. and Minear, J.T., 2014. Dams on the Mekong: Cumulative sediment starvation. *Water Resources Research*, *50*(6), pp.5158-5169.

Le Xuan, T., Ba, H.T., Le Manh, H., Do Van, D., Nguyen, N.M., Wright, D.P., Bui, V.H., Mai, S.T. and Anh, D.T., 2020. Hydraulic performance and wave transmission through pile-rock breakwaters. *Ocean Engineering*, *218*, p.108229.

Le Xuan, T., Le Manh, H., Ba, H.T., Do Van, D., Vu, H.T.D., Wright, D., Bui, V.H. and Anh, D.T., 2022. Wave energy dissipation through a hollow triangle breakwater on the coastal Mekong Delta. *Ocean Engineering*, *245*, p.110419.

Le Xuan, T., Thanh, V.Q., Reyns, J., Van, S.P., Anh, D.T., Dang, T.D. and Roelvink, D., 2019. Sediment transport and morphodynamical modeling on the estuaries and coastal zone of the Vietnamese Mekong Delta. *Continental Shelf Research*, *186*, pp.64-76.

Li, X., Liu, J.P., Saito, Y. and Nguyen, V.L., 2017. Recent evolution of the Mekong Delta and the impacts of dams. *Earth-Science Reviews*, *175*, pp.1-17.

Lovelock, C.E., Cahoon, D.R., Friess, D.A., Guntenspergen, G.R., Krauss, K.W., Reef, R., Rogers, K., Saunders, M.L., Sidik, F., Swales, A. and Saintilan, N., 2015. The vulnerability of Indo-Pacific mangrove forests to sea-level rise. *Nature*, *526*(7574), pp.559-563.

Luijendijk, A., Hagenaars, G., Ranasinghe, R., Baart, F., Donchyts, G. and Aarninkhof, S., 2018. The state of the world's beaches. *Scientific reports*, *8*(1), pp.1-11.

Manh, N.V., Dung, N.V., Hung, N.N., Merz, B. and Apel, H., 2014. Large-scale suspended sediment transport and sediment deposition in the Mekong Delta. *Hydrology and Earth System Sciences*, *18*(8), pp.3033-3053.

Mansard, E.P. and Funke, E.R., 1980. The measurement of incident and reflected spectra using a least squares method. In *Coastal Engineering 1980* (pp. 154-172).

Mentaschi, L., Vousdoukas, M.I., Pekel, J.F., Voukouvalas, E. and Feyen, L., 2018. Global long-term observations of coastal erosion and accretion. *Scientific reports*, *8*(1), pp.1-11.

Meselhe, E., Roelvink, D., Wackerman, C., Xing, F. and Thanh, V.Q., 2017. Modeling the process response of coastal and deltaic systems to human and global changes: Focus on the Mekong system. *Oceanography*, *30*(3), pp.84-97.

Minderhoud, P.S., Hlavacova, I., Kolomaznik, J. and Neussner, O., 2020. Towards unraveling total subsidence of a mega-delta–the potential of new PS InSAR data for the Mekong delta. *Proceedings of the International Association of Hydrological Sciences*, *382*, pp.327-332.

Minderhoud, P.S.J., Erkens, G., Pham, V.H., Bui, V.T., Erban, L., Kooi, H. and Stouthamer, E., 2017. Impacts of 25 years of groundwater extraction on subsidence in the Mekong delta, Vietnam. *Environmental research letters*, *12*(6), p.064006.

Neves, A.C., Gomes, F.V. and Pinto, F.T., 2007. Analysis of the wave-flow interaction with submerged breakwaters. *WIT Transactions on Modelling and Simulation*, *46*.

Ogston, A.S., Allison, M.A., Mullarney, J.C. and Nittrouer, C.A., 2017. Sediment-and hydro-dynamics of the Mekong Delta: From tidal river to continental shelf. *Continental Shelf Research*, *147*, pp.1-6.

Oumeraci, H., 1994a. Review and analysis of vertical breakwater failures—lessons learned. *Coastal engineering*, *22*(1-2), pp.3-29.

Oumeraci, H., 1994b. Scour in front of vertical breakwaters – review of problems. Proc. Int. Workshop on Wave Barriers in Deepwaters, PHRI, Japan, 281-307

Oumeraci, H., 2010. Nonconventional wave damping structures. In *Handbook of Coastal and Ocean Engineering* (pp. 287-315).

Powell, K. and Whitehouse, R.J.S., 1998, July. The occurrence and prediction of scour at coastal and estuarine structures. In *Proceedings of the 33rd MAFF Conference of River and Coastal Engineers*, *Keele University, UK*.

Phan, M.H. and Stive, M.J., 2022. Managing mangroves and coastal land cover in the Mekong Delta. *Ocean & Coastal Management*, *219*, p.106013.

Phan, L.K., van Thiel de Vries, J.S. and Stive, M.J., 2015. Coastal mangrove squeeze in the Mekong Delta. *Journal of Coastal Research*, *31*(2), pp.233-243.

Soulsby, R., 1997. Dynamics of marine sands. Thomas Telford Publishing Ltd. London, United Kingdom.

SIWRR, 2018. Erosion process in the Lower Mekong Delta Coastal Zones (LMDCZ) and measures for protecting Go-Cong and U-Minh from coastal erosion

Thanh, Q.V., 2021. Modeling of hydrodynamics and sediment transport in the Mekong Delta. CRC Press.

Thanh, V.Q., Reyns, J., Wackerman, C., Eidam, E.F. and Roelvink, D., 2017. Modelling suspended sediment dynamics on the subaqueous delta of the Mekong River. *Continental Shelf Research*, *147*, pp.213-230.

Tran, V.T., Nguyen, H.H., Pham, D.H., Nguyen, D.N. and Nguyen, T.T., 2018, November. Hollow cylinder breakwater for dissipation of wave energy to protect the west coast of Ca Mau Province in Vietnam. In *Vietnam Symposium on Advances in Offshore Engineering* (pp. 599-605). Springer, Singapore.

Tuan, T. Q., and Luan, M.T., 2022. Laboratory study of wave damping by porous breakwaters on mangrove mudflats in the Mekong River Delta. *Ocean Engineering*, 258, p. 111846.

Van Binh, D., Kantoush, S. and Sumi, T., 2020. Changes to long-term discharge and sediment loads in the Vietnamese Mekong Delta caused by upstream dams. *Geomorphology*, *353*, p.107011.

Williams, A.T., Rangel-Buitrago, N., Pranzini, E. and Anfuso, G., 2018. The management of coastal erosion. *Ocean & coastal management*, *156*, pp.4-20.

Winterwerp, J.C., Albers, T., Anthony, E.J., Friess, D.A., Mancheño, A.G., Moseley, K., Muhari, A., Naipal, S., Noordermeer, J., Oost, A. and Saengsupavanich, C., 2020. Managing erosion of mangrove-mud coasts with permeable dams–lessons learned. *Ecological Engineering*, *158*, p.106078.

Xing, F., Meselhe, E.A., Allison, M.A. and Weathers III, H.D., 2017. Analysis and numerical modeling of the flow and sand dynamics in the lower Song Hau channel, Mekong Delta. *Continental Shelf Research*, *147*, pp.62-77.

Zanuttigh, B., van der Meer, J.W. 2008. Wave reflection from coastal structures in design conditions. Coastal Engineering (55). 2008. pp. 771-779.

Zelt, J.A. and Skjelbreia, J.E., 1992. Estimating incident and reflected wave fields using an arbitrary number of wave gauges. *Proc. 23rd Int. Conf. Coastal Eng.*, ASCE, pp. 777-789.

Zyserman, J.A. and Johnson, H.K., 2002. Modelling morphological processes in the vicinity of shore-parallel breakwaters. *Coastal Engineering*, *45*(3-4), pp.261-284.

Appendix A

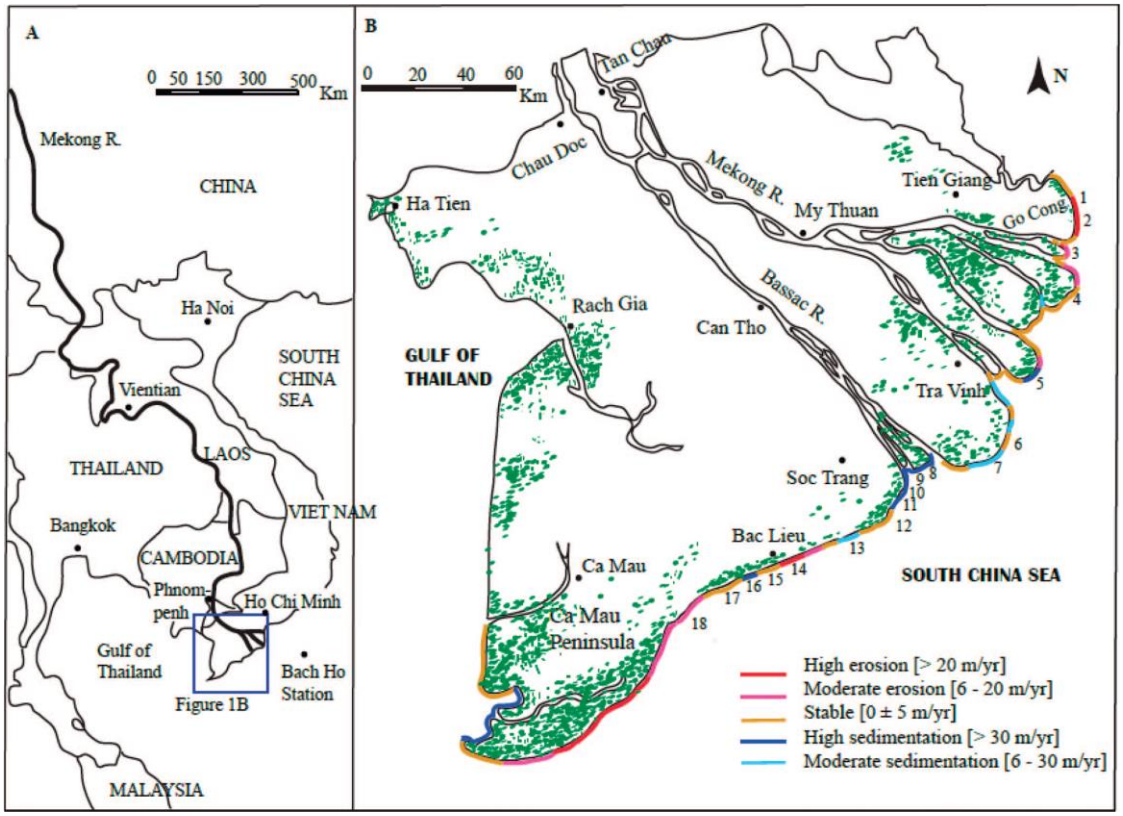
A
0 50 150 300 500 Km
Mekong R.
CHINA
Ha Noi
SOUTH CHINA SEA
Vientian
LAOS
THAILAND
VIET NAM
Bangkok
CAMBODIA
Phnom-penh
Ho Chi Minh
Gulf of Thailand
Bach Ho Station
Figure 1B
MALAYSIA
B
0 20 40 60 Km
N
Tan Chau
Chau Doc
Mekong R.
Tien Giang
My Thuan
Go Cong
Ha Tien
Rach Gia
Bassac R.
Can Tho
GULF OF THAILAND
Tra Vinh
Soc Trang
Bac Lieu
Ca Mau
Ca Mau Peninsula
SOUTH CHINA SEA
1
2
3
4
5
6
7
8
9
10
11
12
13
14
15
16
17
18
High erosion [> 20 m/yr]
Moderate erosion [6 - 20 m/yr]
Stable [0 ± 5 m/yr]
High sedimentation [> 30 m/yr]
Moderate sedimentation [6 - 30 m/yr]

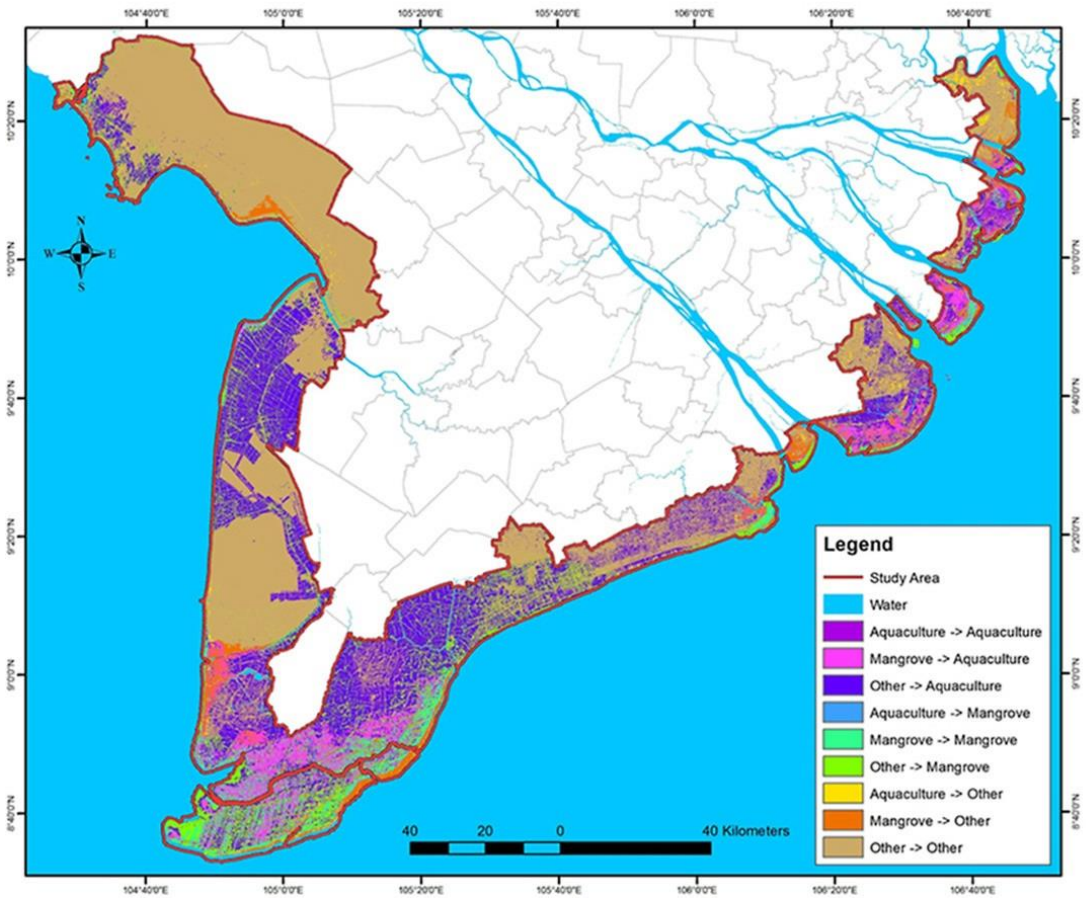

Figure A1. Mangrove forest distribution along the Mekong coast (Phan et al. 2015 (top); Phan and Stive, 2022 (bottom))

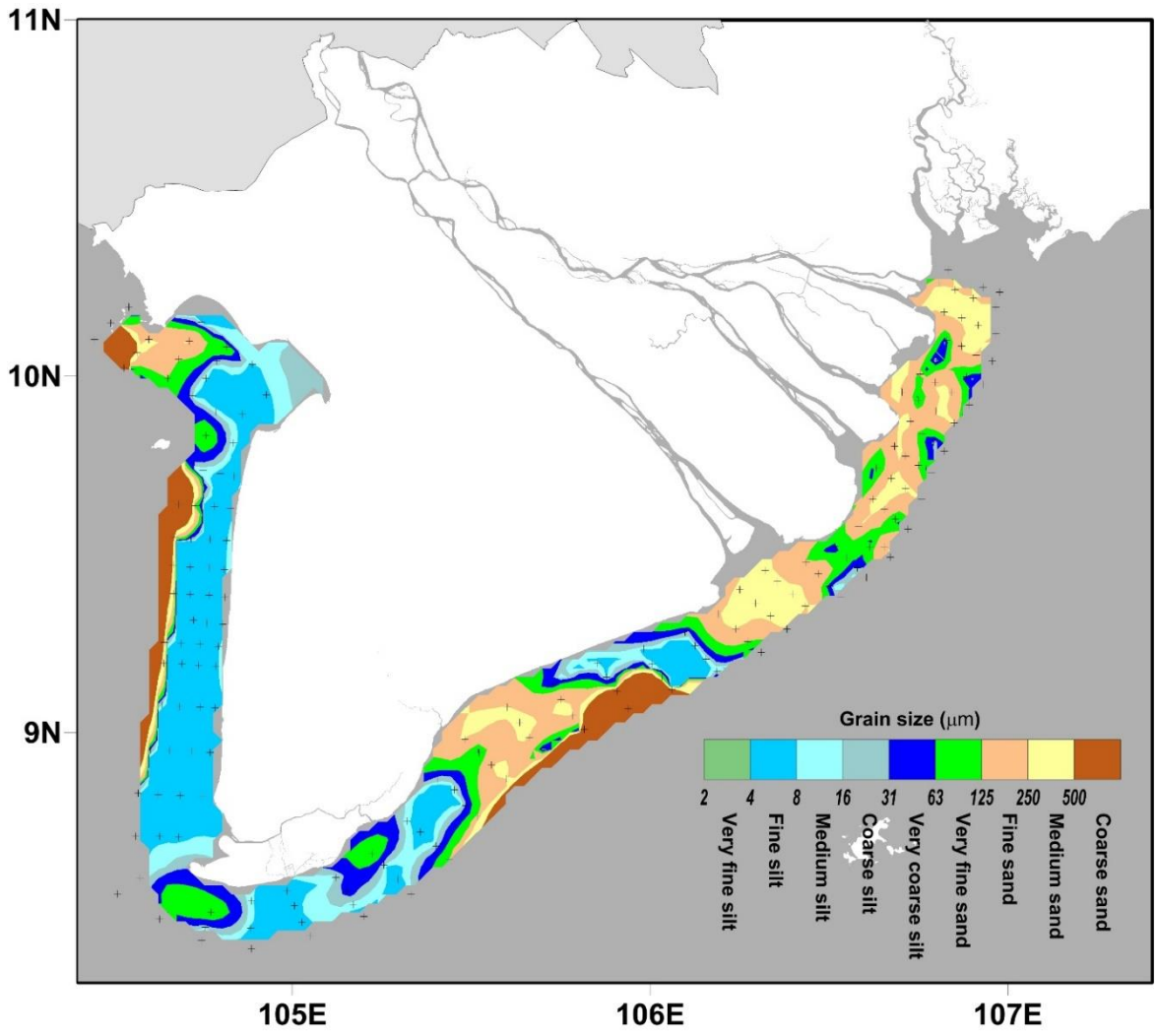

Figure *A*2. Distribution map of the sediment particle size in coastal area of *Vietnamese* M*ekong* D*elta* (Results report of LMDCZ project)

(a)

(b)

Figure A3. The fine sand and mud sediment in East coast of Mekong Delta, at a) Ganh Hao coast, Bac Lieu province, (b) Pile-rock breakwater on Duyen Hai coast, Tra Vinh province